ЖЭТФ, 2012, том 142, вып. 3 (9), стр. 574–593

HALL AND TRANSVERSE EVEN EFFECTS IN THE VICINITY OF A QUANTUM CRITICAL POINT IN $\mathbf{Tm_{1-x}Yb_xB_{12}}$

N. E. Sluchanko [a*], ***A. N. Azarevich*** [a], ***A. V. Bogach*** [a], ***V. V. Glushkov*** [a,b], ***S. V. Demishev*** [a,b], ***M. A. Anisimov*** [a], ***A. V. Levchenko*** [c], ***V. B. Filipov*** [c], ***N. Yu. Shitsevalova*** [c]

[a] *Prokhorov General Physics Institute, Russian Academy of Sciences 119991, Moscow, Russia*

[b] *Moscow Institute of Physics and Technology 141700, Dolgoprudnyi, Moscow Region, Russia*

[c] *Frantsevich Institute for Problems of Materials Science, National Academy of Sciences of Ukraine 03680, Kiev, Ukraine*

Received July 19, 2011,
revised version March 12, 2012

The angular, temperature, and magnetic field dependences of the resistance recorded in the Hall effect geometry are studied for the rare-earth dodecaboride $\mathrm{Tm_{1-x}Yb_xB_{12}}$ solid solutions where the metal–insulator and antiferromagnetic–paramagnetic phase transitions are observed in the vicinity of the quantum critical point $x_c \approx 0.3$. The measurements performed on high-quality single crystals in the temperature range 1.9–300 K for the first time allow revealing the appearance of the second harmonic contribution, a transverse even effect in these fcc compounds near the quantum critical point. This contribution is found to increase drastically both under the Tm-to-ytterbium substitution in the range $x > x_c$ and with an increase in the external magnetic field. Moreover, as the Yb concentration x increases, a negative peak of a significant amplitude appears on the temperature dependences of the Hall coefficient $R_H(T)$ for the $\mathrm{Tm_{1-x}Yb_xB_{12}}$ compounds, in contrast to the invariable behavior $R_H(T) \approx$ const found for $\mathrm{TmB_{12}}$. The complicated activation-type behavior of the Hall coefficient is observed at intermediate temperatures for $x \geq 0.5$ with activation energies $E_g/k_B \approx 200$ K and $E_a/k_B = 55$–75 K, and the sign inversion of $R_H(T)$ is detected at liquid-helium temperatures in the coherent regime. Renormalization effects in the electron density of states induced by variation of the Yb concentration are analyzed. The anomalies of the charge transport in $\mathrm{Tm_{1-x}Yb_xB_{12}}$ solid solutions in various regimes (charge gap formation, intra-gap many-body resonance, and coherent regime) are discussed in detail and the results are interpreted in terms of the electron phase separation effects in combination with the formation of nanosize clusters of rare earth ions in the cage-glass state of the studied dodecaborides. The data obtained allows concluding that the emergence of Yb–Yb dimers in the $\mathrm{Tm_{1-x}Yb_xB_{12}}$ cage-glass matrix is the origin of the metal–insulator transition observed in the achetypal strongly correlated electron system $\mathrm{YbB_{12}}$.

1. INTRODUCTION

Hall effect measurements are usually considered one of key experiments to reveal a transformation of the electron excitation spectrum in the vicinity of a quantum critical point (QCP) [1, 2]. Recently, the anomalies of the Hall coefficient were observed in various systems near an antiferromagnetic (AF) QCP (at the Néel temperature $T_N = 0$), which corresponds to the transition from the antiferromagnetic to paramagnetic state in heavy-fermion systems with metallic conductivity [3–6]. Because the magnetic order in heavy-fermion metals is usually attributed to the onset of a magnetic structure of the localized magnetic moments of rare-earth ions, the considered antiferromagnetic–paramagnetic transition from the magnetic to nonmagnetic heavy-fermion ground state through the QCP may be simultaneously accompanied by delocalization of the electronic states of the rare-earth ions.

In the ongoing discussion on the nature of the electron structure transformation in rare-earth compounds

*E-mail: nes@lt.gpi.ru

in the nearest vicinity of the QCP, two possible scenarios of the quantum phase transition are analyzed most actively. According to the first approach, the localized magnetic moments of rare-earth ions at the QCP are coupled to itinerant electrons in the many-body states, such that these heavy fermions form antinodes of the spin-density wave in the metallic matrix [7–9]. In the alternative scenario, an abrupt change in the Fermi surface volume occurring at the QCP owing to the decay of many-body states causes an "unfreezing" of the localized magnetic moments of the rare-earth ions [1, 9]. The third, quite different approach to the interpretation of charge transport anomalies in substitutional solid solutions $CeCu_{6-x}Au_x$ was recently proposed in [6], where the Hall effect was studied in detail in the vicinity of the AF QCP $x_c \approx 0.1$. In particular, along with a remarkable increase in the Hall coefficient near the QCP, the appearance of even harmonics (in magnetic field) in the Hall resistance observed in [6] was attributed to the occurrence of electron-type phase separation in these heavy fermion compounds in the vicinity of the QCP. Keeping in mind the examples of the systems with fast $4f$–$5d$ spin fluctuations and the AF QCP in which the metal–insulator and antiferromagnetic–paramagnetic transitions occur simultaneously, it is of interest to investigate the Hall effect features in the vicinity of the AF QCP with the metal–insulator transition.

One of the most convenient compounds for these test experiments is the $Tm_{1-x}Yb_xB_{12}$ system, where the thulium-to-ytterbium substitution causes the development of an AF instability in approaching the QCP at $x = x_c \approx 0.3$ [10] and the metal–insulator transition is observed in a wide vicinity of the QCP. Neutron diffraction studies of TmB_{12} have shown that within experimental resolution, the magnetic structure of the antiferromagnet (Néel temperature $T_N \approx 3.2$ K [10–12]) can be well described as an incommensurate one with the propagation vector $\mathbf{q} = (1/2 + \delta, 1/2 + \delta, 1/2 + \delta)$, where $\delta = 0.035$–0.038 [11, 12]. The continuous metal–insulator transition occurs in the $Tm_{1-x}Yb_xB_{12}$ series in the concentration range $0 < x \leq 1$ and is accompanied by a huge ($\sim 10^7$ times) increase in resistivity from 4 $\mu\Omega$·cm (TmB_{12}) and 10 Ω·cm (YbB_{12}) [10, 13]. It is worth noting here that according to the results of Seebeck coefficient measurements [10] in the range $x \leq 0.3$, the activation energy $E_g/2$ on the magnetic side of the antiferromagnetic–paramagnetic transition increases drastically from zero in the antiferromagnetic metal TmB_{12}. Above x_c, the deduced value $E_g/k_B = 120$–160 K [10] becomes approximately equal to the band gap obtained from the charge transport [13], NMR [14], and heat-capacity measurements [15] for the YbB_{12} narrow-gap semiconductor with strong charge and spin fluctuations.

We note that the main contribution to the electronic relaxation time τ in these Yb-based dodecaborides is the scattering of charge carriers by fast $4f$–$5d$ charge and spin fluctuations with $\tau \sim 10^{-13}$ s [16]. At the same time, the effective masses determined from the quantum oscillations are not very large, $m^* = (0.5$–$1.2)m_0$ [17]. As a result, in the case of $Tm_{1-x}Yb_xB_{12}$ compounds, the magnetic fields $\mu_0 H \leq 10$ T correspond to the low-field limit of galvanomagnetic effects. These properties are measured under the condition $\omega_c\tau < 1$ (where ω_c is the cyclotron frequency), which implies that each itinerant electron can only complete a very short segment of its cyclotron orbit during its mean free lifetime between collisions.

It is also worth noting that a nearly temperature-independent behavior of the Hall coefficient was found previously for all metallic dodecaborides RB_{12} (R = = Ho, Er, Tm, Lu) with sufficiently small negative values $R_H = -(3$–$4)\cdot 10^{-4}$ cm^3/C [18]. Furthermore, both of the optical conductivity measurements [19] and the band structure calculations [20–23] have allowed estimating the plasma frequency $\hbar\omega_{pl} \approx 1.6$ eV at room temperature for YbB_{12} and the nonmagnetic reference compound LuB_{12}. The relatively high value of ω_{pl} identifies the dodecaborides as good metals with a conduction band, which is constructed predominantly from $5d$ states of the rare earth ions hybridized with boron $2p$ orbitals. Recently, precision measurements of the specific heat and Hall effect, as well as detailed studies of low-temperature Raman spectra were performed on single crystals of the nonmagnetic reference compound lutetium dodecaboride with various boron isotope compositions, indicating the formation of a disordered cage-glass state in LuB_{12} at liquid-nitrogen temperatures [24, 25]. Taking the similarity of the crystal and electronic structures of LuB_{12} and YbB_{12} into account, it is natural to expect that the disordering effects are essential in the formation of the insulating ground state in this archetypal strongly correlated electron system, the narrow-gap semiconductor YbB_{12}.

The main goal of this work is therefore to carefully investigate the Hall effect in $Tm_{1-x}Yb_xB_{12}$ compounds with the AF QCP and metal–insulator transition. Moreover, an extraordinarily strong transverse even effect has been detected and analyzed recently [6] in the archetypal heavy hermion compounds $CeCu_{6-x}Au_x$ in the vicinity of the AF QCP ($x = 0.1$). To investigate both these odd and even transverse voltages in the Hall effect geometry in the series of $Tm_{1-x}Yb_xB_{12}$, the sam-

ple rotation technique developed about 40 years ago (see [26] and references therein) is applied in this study (see experimental details below).

As a result of the study of the Hall and even transverse effects in the series of $Tm_{1-x}Yb_xB_{12}$ solid solutions, we here answer two important questions about (i) the nature of the gap in the so-called Kondo insulator YbB_{12} and (ii) the origin of the intra-gap states in this archetypal narrow-gap semiconductor with strong electron correlations. It is shown below that the appropriate scenario of the gap opening in these RB_{12} conductors is based on the formation of R^{3+}–R^{3+} dimers in the matrix of $Tm_{1-x}Yb_xB_{12}$. In more detail, the formation of randomly disposed dimers with the size $a_{p1} \approx 5$ Å is argued to be the reason of the local gap (on the scale of the RB_{12} unit cell with $E_g \approx 18$ meV) emerging near the Fermi energy E_F in the conduction band of these compounds. Additionally, the intra-gap many-body resonance developed in $Tm_{1-x}Yb_xB_{12}$ at E_F is deduced for the first time from the Hall effect measurements together with the second harmonic term (transverse even effect), which is caused by the effect of electronic phase separation.

2. EXPERIMENTAL DETAILS

In the present study, the angular, temperature, and magnetic-field dependences of the resistance $\rho_H(\varphi, H_0, T_0)$ from the Hall probes and the resistivity $\rho(T)$ are investigated for substitutional solid solutions $Tm_{1-x}Yb_xB_{12}$ in the range of compositions $0 \le x \le 0.81$ at temperatures in the interval 1.9–300 K in magnetic fields up to 8 T. The measurements were performed on high-quality single crystals of rare-earth dodecaborides.

2.1. Samples investigated

The single crystals of $Tm_{1-x}Yb_xB_{12}$ solid solutions were prepared in a multistage process consisting of (i) synthesis of the source powders, (ii) their compacting and sintering into rods, and (iii) growth of the single crystals by inductive zone melting. At each stage, the single-phase state of the product was verified by X-ray diffraction and other experimental techniques. The $Tm_{1-x}Yb_xB_{12}$ source powders were synthesized by the reduction of a mixture of the thulium and ytterbium metal oxides taken in the corresponding ratio in the presence of boron at 1900 K in a vacuum according to the routine reaction

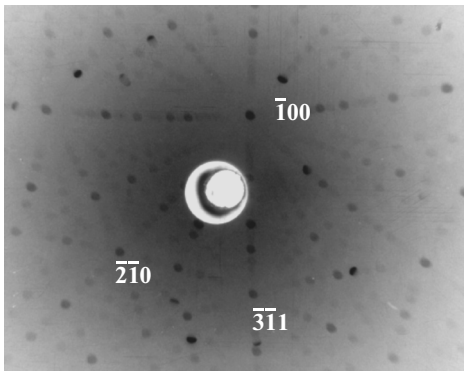

Fig. 1. X-ray Laue pattern from the lateral cross section of a raw single crystal with the nominal composition $Tm_{0.75}Yb_{0.25}B_{12}$. Deviation of the growth direction from [100] is about 10°

$$(1-x)Tm_2O_3 + xYb_2O_3 + 27B \rightarrow \rightarrow 2Tm_{1-x}Yb_xB_{12} + 3BO\uparrow$$

$$(0 \le x \le 0.81).$$

The respective content of the main substance in the initial Tm_2O_3 and Yb_2O_3 oxides was 99.986 and 99.998 wt. %, and this content in the initial amorphous boron powder was higher than 99.5 wt. %. The highly volatile impurities present in boron were deleted in two stages: (i) during the synthesis procedure and, after that, (ii) in the zone melting process.

The undertaken X-ray phase analysis has shown that the synthesized powders are single-phase product, i. e., the compositions $Tm_{1-x}Yb_xB_{12}$ ($0 < x \le 0.81$) constitute a continuous series of solid solutions with the crystal structure of the UB_{12} type. The resulting powders were then coldmolded into rods (8 mm in diameter and 60 mm in length), which were sintered in a vacuum at temperatures about 2000 K. A crucible-free inductive floating zone melting was applied to grow $Tm_{1-x}Yb_xB_{12}$ single crystals using the special unit Crystal-111 at the Institute for Problems of Materials Science, National Academy of Sciences of Ukraine (Kiev).

The main problem to be solved here was to grow single crystals without the precipitation of foreign phases with the permanent Tm/Yb ratio kept both along the growing axis and in the lateral cross section of crystals. Taking difference in both the vapor pressure of Tm and Yb metals and their distribution coefficients into account, we optimized the gas pressure (highly pure Ar, $P \le 1.5$ MPa), the crystallization rate (0.2–1 mm/min), the speed of rotation of feed and growing rods (0–10 rpm), the starting displacement

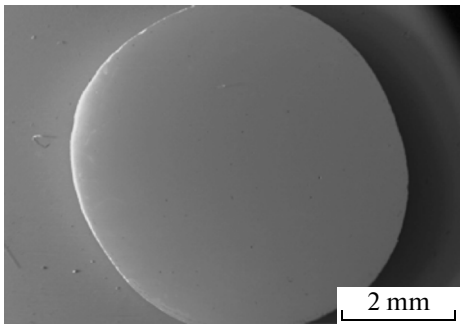

Fig. 2. General view of the lateral cross section of the single crystal with the nominal composition $Tm_{0.75}Yb_{0.25}B_{12}$

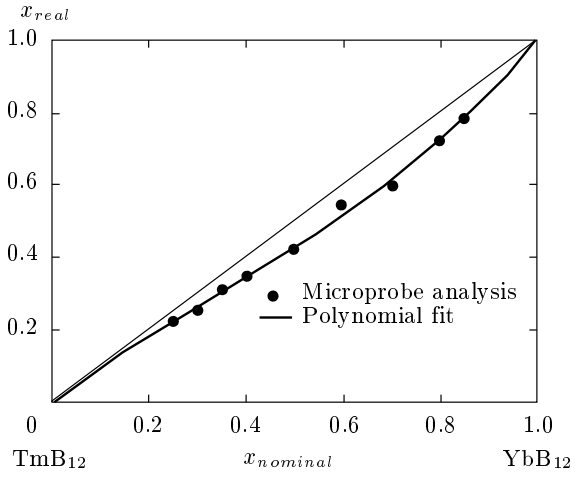

Fig. 3. Real Tm/Yb ratios versus nominal ones for $Tm_{1-x}Yb_xB_{12}$ single crystals

of the zone composition from stoichiometry by boron piece introduction, and so on for each $Tm_{1-x}Yb_xB_{12}$ composition. In the process of optimization of the growth technology, Laue back patterns were used for primary analysis of the crystal structure quality. The technology worked through in such a way in order to avoid the splitting of point reflections in the Laue pattern that corresponds to the lack of misorientation of blocks in the limit of several tenths of degree (procedure resolution) (Fig. 1). As a result, single crystals of all nominal compositions $Tm_{1-x}Yb_xB_{12}$ ($0 \le x \le 0.81$) were grown with diameters of 4–6 mm and a length of about 50 mm. These crystal rods consisted of the single crystal core that was free of block boundaries and was surrounded by a superfine polycrystalline ring (Fig. 2). Electron microscopy showed that second phase inclusions of the CaB_6 or YB_{25} types sometimes appeared at the periphery of the ingot in the lateral cross section. In these cases, the samples for the present study were cut from the central part of oriented polished plates (discs, $h \approx 0.6$–0.8 mm) and, as a result, these foreign inclusions were completely removed from the experimental samples.

The Tm/Yb ratio was estimated for all $Tm_{1-x}Yb_xB_{12}$ single crystals using a scanning electron microscope equipped with a system of the energy dispersion microprobe (REM-106; the electron probe size is about 2 μm^2). The measurements were carried out at several points of the lateral cross section (periphery $r = 1$, middle $r = 1/2$, and center $r = 0$) on both sides of the single crystal rods to be sure that the Tm/Yb ratio is invariant. In these experiments, the individual metals (Tm, Yb) and individual binary borides (TmB_{12}, YbB_{12}) were used as reference samples; it was shown that the results of this analysis for the same sample in the case of both types of reference samples are identical. The accuracy of the microanalysis was found to be about 1 % when the element concentration was more than 10 % in the compound under investigation. The real composition of the single crystal differs from the source nominal one (Fig. 3) due to the preferential evaporation of Yb from the melting zone. For example, the real composition of the sample with the nominal composition $Tm_{0.75}Yb_{0.25}B_{12}$ is $Tm_{0.77}Yb_{0.23}B_{12}$ and it is invariable for all three points $r = 0$, $1/2$, and 1 studied by microanalysis. Additionally, a spectral optical analysis was used to estimate the concentration of impurities (the total concentration of impurities, except the rare earth elements, did not exceed 10^{-3} wt. %; rare-earth impurities were determined in the source oxides). Finally, the lattice parameters of dodecaborides were estimated from X-ray diffraction measurements in an HZG-4 diffractometer on the crushed single crystals in Cu K_α radiation with a Ni filter (Fig. 4). It follows from the data plotted in Fig. 4 that the lattice parameters of $Tm_{1-x}Yb_xB_{12}$ do not obey Vegard's law.

2.2. Experimental method for the Hall and transverse even effects

To study the Hall and transverse even resistances, the original sample rotation technique was applied with a stepwise fixing of the sample position in the steady magnetic field with the induction **B** that was perpendicular to the measuring direct current $\mathbf{I} \parallel \langle 110 \rangle$ (see inset in Fig. 5, the normal vector $\mathbf{n} \parallel \langle 001 \rangle$). The method is similar to the one applied previously (see, e. g., re-

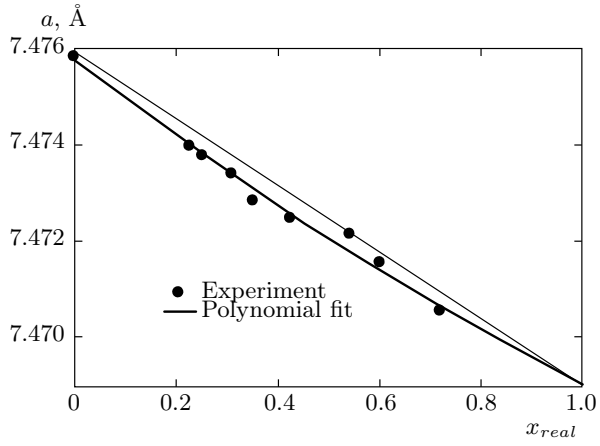

Fig. 4. Lattice parameters versus the real composition of $Tm_{1-x}Yb_xB_{12}$ single crystals

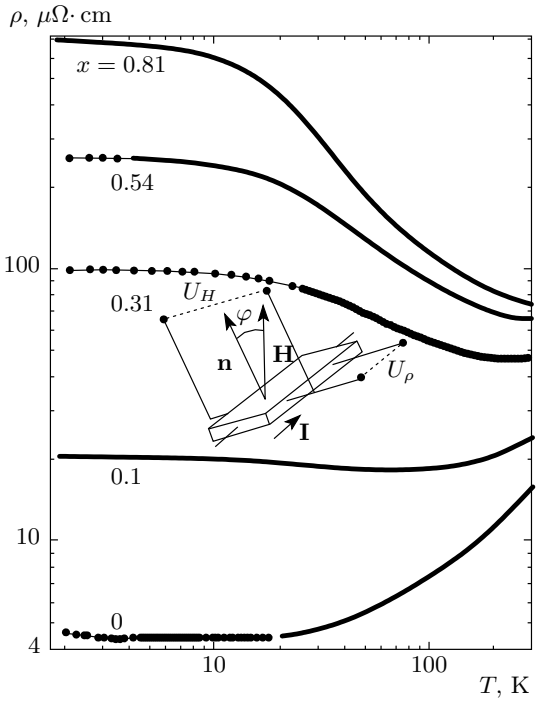

Fig. 5. Temperature dependences of the resistivity for $Tm_{1-x}Yb_xB_{12}$ compounds. The inset shows the scheme of the Hall effect measurements, $\mathbf{n} \parallel \langle 001 \rangle$

view [26]); the installation used previously in [27] was equipped with a step-motor with automated control of the step-by-step sample rotation.

In the method, the single crystalline sample lies in the xy plane while $\mathbf{B}$ may be scanned in the yz plane about the x axis. The expression for the Hall field in a noncubic metal is [26]

$$E_{Hall} = \frac{I_x}{2}\left[\rho_{yx}(\mathbf{B}) - \rho_{xy}(\mathbf{B})\right]\cos\varphi + \frac{I_x}{2}\left[\rho_{zx}(\mathbf{B}) - \rho_{xz}(\mathbf{B})\right]\sin\varphi \quad (1)$$

or, with a less cumbersome notation for the antisymmetric part of the resistivity tensor

$$\rho^a_{ik}(\mathbf{B}) = R^{(1)}_{ikp}B_p \quad (i,k,p = \{x,y,z\}),$$

it can be rewritten as

$$E_{Hall} = R_1 IB\cos\varphi + R_2 IB\sin\varphi. \quad (2)$$

In the case of a cubic metal, the equality $R_2 = 0$ is valid and relations (1) and (2) simplify to the cosine-type dependence. Hence, the appearance of any anisotropy type in the Hall field can be verified by the emergence of the second term in the right-hand side of Eqs. (1) and (2); as a result, $E_{Hall}(\varphi)$ becomes effectively phase-shifted along the φ axis by the angle φ_0 whose value satisfies the relation $\mathrm{tg}\,\varphi_0 = R_1/R_2$.

In the experiment with the sample rotation in a magnetic field, simultaneously with the Hall field measurements, another component of the total electric field in a metal is recorded which is well known as the transverse even (TE) effect and which lies in a direction transverse to the primary current. The TE effect is an even function of $\mathbf{B}$ and it is different from both the transverse magnetoresistance and TE planar effect [26]. This even transverse field is given by Eq. (1) for the symmetric part of the resistivity tensor

$$\rho^s_{ik}(\mathbf{B}) = \rho^{(0)}_{ik} + R^{(2)}_{ikpq}B_pB_q \quad (i,k,p,q = \{x,y,z\})$$

and can be rewritten as [26]

$$E_{TE} = \frac{I_x}{2}\left[\rho_{yx}(\mathbf{B}) + \rho_{xy}(\mathbf{B})\right]\cos\varphi + \frac{I_x}{2}\left[\rho_{zx}(\mathbf{B}) + \rho_{xz}(\mathbf{B})\right]\sin\varphi. \quad (3)$$

For an isotropic metal, whenever $\mathbf{B}$ coincides with the z direction, $\rho_{zx}(\mathbf{B}) = \rho_{xz}(\mathbf{B}) = 0$ (see [26]) and Eq. (3) simplifies considerably. Moreover, unless the conductivity is anisotropic in the xy plane, the first term in the right-hand side of Eq. (3), $\rho_{yx}(\mathbf{B}) + \rho_{xy}(\mathbf{B})$, is also zero. To summarize, for paramagnetic $Tm_{1-x}Yb_xB_{12}$ compounds with the fcc crystal structure, the only cosine-type contribution to the Hall resistivity ρ_H in the measurements of the signal from the Hall probes should appear in the low-field limit $\omega_c\tau < 1$.

2.3. Estimation of the transverse magnetoresistance contribution

In the study, special attention was paid to the symmetric location of the Hall probes to minimize the con-

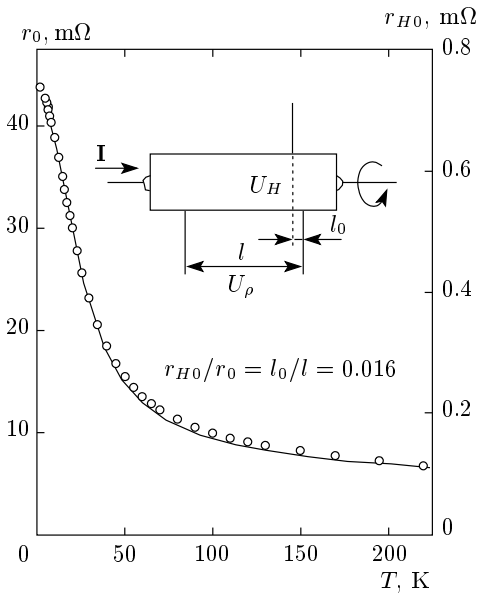

Fig. 6. Temperature dependences of the angular invariable components in (i) the Hall resistance (constant bias r_{H0}, open circles) and (ii) magnetoresistance (r_0, solid line), respectively measured from the Hall and potential probes for the $Tm_{0.28}Yb_{0.72}B_{12}$ sample. The inset shows the scheme of the 5-probe resistive measurements (**I** is the measuring current; l, U_ρ and l_0, U_H are the distances and voltages between the potential and Hall probes)

tribution from the negative magnetoresistance. We emphasize that the transverse configuration used here for measurements of the Hall and transverse even effects (the axis of the sample rotation being parallel to the direction of the measuring current **I** and perpendicular to **H**; see the scheme in the inset in Fig. 5) eliminates the contribution from the longitudinal magnetoresistance to the Hall signal [6, 27]. At the same time, careful alignment of the Hall probes mounted to the samples studied (see inset in Fig. 6) is very important in order to minimize the transverse magnetoresistance contribution to the Hall voltage. An example of a quantitative analysis of the magnitudes of these two transverse contributions is presented in the next section for the $Tm_{0.28}Yb_{0.72}B_{12}$ solid solution. It is shown below that the contribution from the conventional transverse magnetoresistance to the signal measured from the Hall probes does not exceed 6 % of the real measured Hall resistance in $Tm_{1-x}Yb_xB_{12}$ in the magnetic field up to 8 T.

3. RESULTS AND DISCUSSION

3.1. Resistivity

The results of the resistivity measurements $\rho(T)$ on the $Tm_{1-x}Yb_xB_{12}$ samples with various Yb contents are presented in Fig. 5. According to the data in Fig. 5, the $\rho(T)$ dependence for antiferromagnet TmB_{12} ($x = 0$, $T_N = 3.2$ K) exhibits a typical metallic behavior with both a significant decrease in the resistivity with a decrease in the temperature and a small enough residual value $\rho_0 \approx 4\ \mu\Omega \cdot$ cm. Thulium-to-ytterbium substitution in $Tm_{1-x}Yb_xB_{12}$ solid solutions with $x < x_c$ is accompanied by both the appearance of a pronounced minimum of the resistivity at temperatures above 12 K and a strong increase in the spin-flip scattering contribution to $\rho(T)$ with an increase in the Yb content. The evolution of the temperature dependences of the resistivity in the wide vicinity of the QCP (Fig. 5) testifies in favor of the metal–insulator transition in the $Tm_{1-x}Yb_xB_{12}$ dodecaborides. Indeed, when x varies in the range $0 \le x \le 0.81$, the resistivity at liquid-helium temperatures increases by more than two orders of magnitude, and the increase cannot be interpreted in terms of the charge carriers' scattering caused by the substitution disorder. On the other hand, we note that no activation behavior of $\rho(T)$ is observed throughout the concentration range $x \le 0.81$.

3.2. Hall resistivity contributions

Below, we use the Hall resistivity term (ρ_H) only to simplify the presentation of the experimental results obtained in the Hall effect geometry, including both the Hall and TE components of resistivity into ρ_H. The misuse of the term in this sense seems to have arisen because in the usual experimental arrangement, the transverse even effect appears between the electrodes normally used to determine the Hall voltage. Although it is therefore superficially like the Hall effect, the TE effect is strictly part of the Ohmic field [26].

The Hall resistivity angular dependences are shown in Figs. 7 and 8 as the typical examples obtained for $Tm_{0.46}Yb_{0.54}B_{12}$ at various temperatures in the magnetic field $\mu_0 H = 1.5$ T and for $Tm_{0.28}Yb_{0.72}B_{12}$ at liquid-helium temperature $T_0 = 2.1$ K for several magnetic field values in the range $\mu_0 H \le 8$ T. We note that except the antiferromagnet TmB_{12} ($T_N = 3.2$ K), all the $Tm_{1-x}Yb_xB_{12}$ samples with the Yb content in the range $0.1 < x \le 0.81$ investigated here are paramagnets at temperatures $T > 1.9$ K. The dodecaborides are crystallized in the fcc structure, and, according to

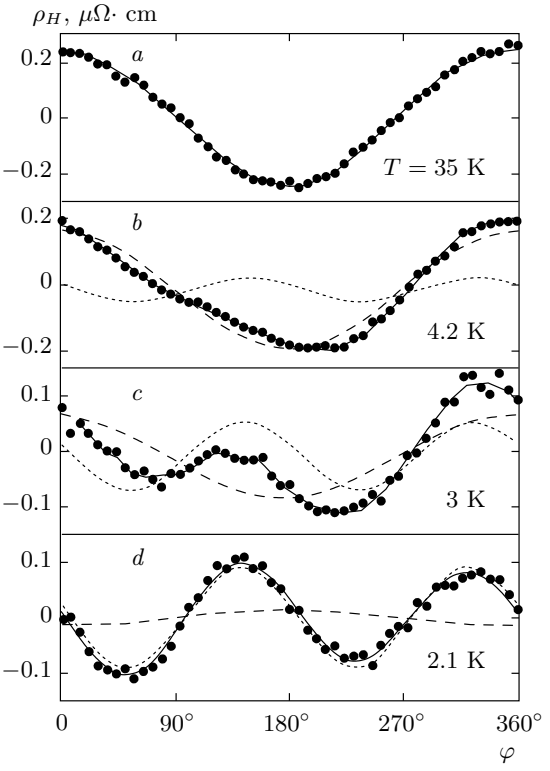

Fig. 7. Angular dependences of the Hall resistivity $\rho_H(\varphi)$ for $Tm_{0.46}Yb_{0.54}B_{12}$ recorded in the magnetic field $\mu_0 H = 1.5$ T at various temperatures in the range 2–35 K. For all $\rho_H(\varphi)$ curves, the decomposition into the odd and even harmonics is presented (see Eq. (1))

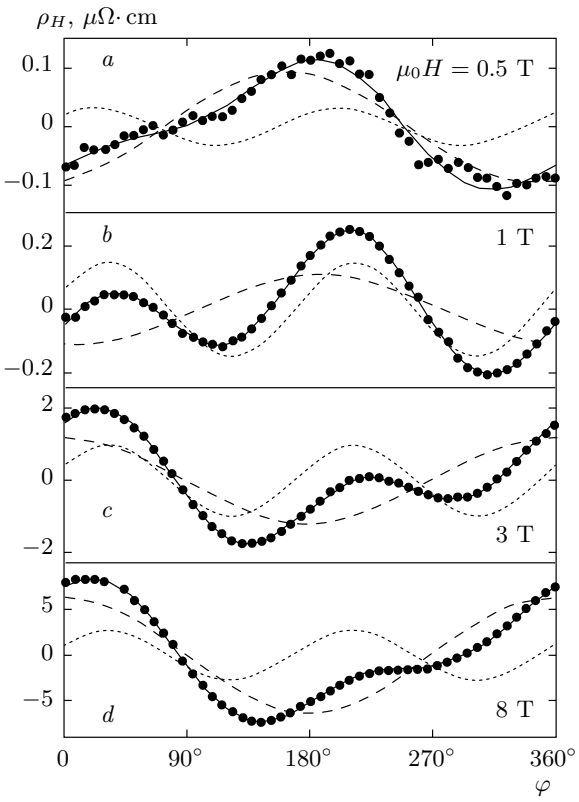

Fig. 8. Angular dependences of the Hall resistivity $\rho_H(\varphi)$ for $Tm_{0.28}Yb_{0.72}B_{12}$ recorded at the liquid-helium temperature $T = 2.1$ K in magnetic fields $\mu_0 H \leq 8$ T. For all $\rho_H(\varphi)$ curves, the decomposition into the odd and even harmonics is presented (see Eq. (1))

Eq. (1), it is reasonable to expect a cosine-type angular dependence of the Hall resistivity, $\rho_H(\varphi) \sim \rho_{H1}\cos\varphi$, when the sample is rotated in the magnetic field (see the inset in Fig. 5). Such a behavior of $\rho_H(\varphi)$ was observed in our experiments for the $Tm_{1-x}Yb_xB_{12}$ solid solutions in the range $0.1 < x < 0.6$ at temperatures above 30 K and in magnetic fields up to 2 T (see, e. g., Fig. 7*a*). Upon a decrease in the temperature in the range $T < 30$ K, a remarkable contribution from the second harmonic appears in the Hall signal (see Figs. 7*b–d* and 8*a–d*).

In this study, we describe the angular dependence of the Hall resistivity $\rho_H(\varphi, T_0, H_0)$ of $Tm_{1-x}Yb_xB_{12}$ solid solutions by the relation

$$\rho_H(\varphi, T_0, H_0) = \rho_{H0} + \rho_{H1}\cos\varphi + \\ + \rho_{H2}\cos(2\varphi - \Delta\varphi), \quad (4)$$

where ρ_{H0} is the constant bias, ρ_{H1} is the Hall effect contribution, and the second harmonic term ρ_{H2}, which is even in the magnetic field, is taken into account with the phase shift $\Delta\varphi$ with respect to the main component of the Hall signal. It is worth noting here that within experimental accuracy, we have not found any phase shift along the φ axis through the angle φ_0 of the main $\rho_{H1}\cos\varphi$ contribution to the Hall effect, concluding opposite to appearance of any type of anisotropy in the Hall field (see Eqs. (1) and (2)). It can be seen in Figs. 7 and 8 that at liquid-helium temperatures for $Tm_{1-x}Yb_xB_{12}$ compounds with the Yb concentration x above the QCP $x_c \approx 0.3$, the amplitude ρ_{H2} of this even component in the Hall resistivity becomes comparable with or considerably exceeds the usual odd cosine contribution $\rho_{H1}(\varphi)$ in magnetic fields $1\text{ T} < \mu_0 H < 3$ T. The sign reversal of the odd component is observed for $x \geq 0.5$ both when the temperature decreases in the range 4.2–1.9 K (cf. Figs. 7*c* and 7*d*) and when the magnetic field increases at $T_0 = 2.1$ K (Figs. 8*b* and 8*c*). Moreover, because of a small but finite phase shift $\Delta\varphi \neq 0$ between the main ρ_{H1} and even

ρ_{H2} components, the positions of the extrema on the experimental curves $\rho_H(\varphi, T_0, H_0)$ disagree with two directions of the normal vector $\mathbf{n}$ (see the inset in Fig. 5, $\varphi = 0$ and $\varphi = 180°$).

In such a situation, the conventional technique typically used for Hall effect studies is not appropriate for the separation and analysis of the Hall resistivity components. Indeed, the conventional technique is based on the measurement of the Hall signal at two values, $\varphi = 0$ and $\varphi = 180°$, of the angle between $\mathbf{n}$ and $\mathbf{H}$ vectors, with the Hall resistivity estimated as the half-difference, $[\rho_H(\varphi = 0) - \rho_H(\varphi = 180°)]/2$, which results in a loss of this even harmonic signal in the final product. Moreover, this evidently leads to an incorrect evaluation of the Hall coefficient for $Tm_{1-x}Yb_xB_{12}$ compounds with the Yb content $x > x_c$ in the case of any small noncollinearity of the $\mathbf{n}$ and $\mathbf{H}$ vectors (see, e. g., Figs. 7 and 8). Thus, the measurements of the $\rho_H(\varphi, T_0, H_0)$ angular dependences and their analysis in the framework based on relation (4) are of crucial importance and are the only correct method to analyze the Hall effect contributions in the $Tm_{1-x}Yb_xB_{12}$ system with the quantum critical point $x_c \approx 0.3$ and a metal–insulator transition.

At the same time, it is crucially important to estimate and compare the magnitudes of (i) the conventional transverse magnetoresistance contribution to the Hall effect and (ii) the Hall resistance itself, both measured in the same experiment with rotation of the sample in the transverse magnetic field (see the insets in Figs. 5 and 6). Indeed, any misalignment of the Hall probes for the length l_0 (see inset in Fig.6) causes the appearance of the portion $U_\rho l_0/l = f(\varphi)$ in the Hall signal $U_H(\varphi)$. To compare these magnitudes, we simultaneously measured both the resistance $r(\varphi) = U_\rho(\varphi, H)/I$ between the potential probes and the Hall resistance $r_H(\varphi) = U_H(\varphi, H)/I$ (Fig. 9). Taking both the constant bias (r_0 and r_{H0}) and angular dependent components (r_2, r_{H1}, and r_{H2}) in these resistances into account (see fits and relations in Fig. 9), it is possible to detect the ratio l_0/l of the distances between the Hall and potential probes from the respective angular invariable components r_0 and r_{H0} in $r(\varphi)$ and $r_H(\varphi)$. Indeed, the constant bias ρ_{H0} in the Hall resistivity $\rho_H(\varphi, T_0, H_0)$ (see Eq. (4)) is proportional to the aforementioned small displacement of the Hall probes at the distance l_0 along the current direction, $\rho_{H0} \sim r_{H0} \sim l_0$, and hence the ratio r_{H0}/r_0 of the resistances is proportional to l_0/l (see the inset in Fig. 6). According to the data plotted in Fig. 6, the proportionality $r_{H0}/r_0 = \text{const}$ holds with a good accuracy in the entire temperature range 2–300 K; as a result,

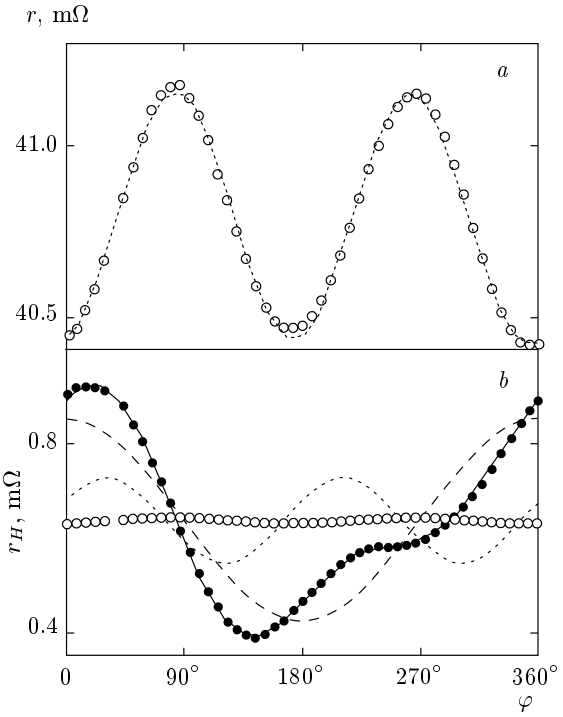

Fig. 9. Angular dependences of (a) the magnetoresistance $r(\varphi) = r_0 + r_2(\varphi)$, $r_0 = 4.08 \cdot 10^{-2}$, $r_2 = 3.64 \cdot 10^{-4}$ and (b) the Hall resistance $r_H(\varphi) = r_{H0} + r_{H1}(\varphi) + r_{H2}(\varphi)$, $r_{H0} = 6.38 \cdot 10^{-4}$, $r_{H2} = 9.68 \cdot 10^{-5}$ for $Tm_{0.28}Yb_{0.72}B_{12}$ as recorded at the liquid-helium temperature $T = 2.1$ K in the magnetic field $\mu_0 H = 8$ T. For all $r(\varphi)$ and $r_H(\varphi)$ curves, the decomposition into the odd and even harmonics is presented and the amplitudes r_0, r_2 and r_{H0}, r_{H1}, r_{H2} are deduced (see Eq. (1)). The estimated contribution to the Hall resistance from the transverse magnetoresistance is also shown in the lower panel (open circles)

the ratio of the lengths is estimated as $l_0/l = 0.016$. Then, in the analysis of the second harmonic amplitudes, both in the transverse magnetoresistance $r(\varphi)$ and in the Hall resistance $r_H(\varphi)$ (see the parameters r_2 and r_{H2} in the caption to Fig. 9), it is evident from the ratio $(r_2/r_{H2})l_0/l \approx 0.06$ that the magnetoresistance component measured from the Hall probes does not exceed 6 % of the even contribution to the Hall signal (see the curve and open circles in Fig. 9b). It is worth noting that this "upper limit" estimate was carried out in the highest magnetic field used in this study ($\mu_0 H = 8$ T) and for the $Tm_{0.28}Yb_{0.72}B_{12}$ sample at lowest temperatures (near 2 K), where the transverse magnetoresistance effect is one of the largest in the family of $Tm_{1-x}Yb_xB_{12}$ solid solutions with ytterbium concentration in the range $0.3 < x \leq 0.81$. Hence, it

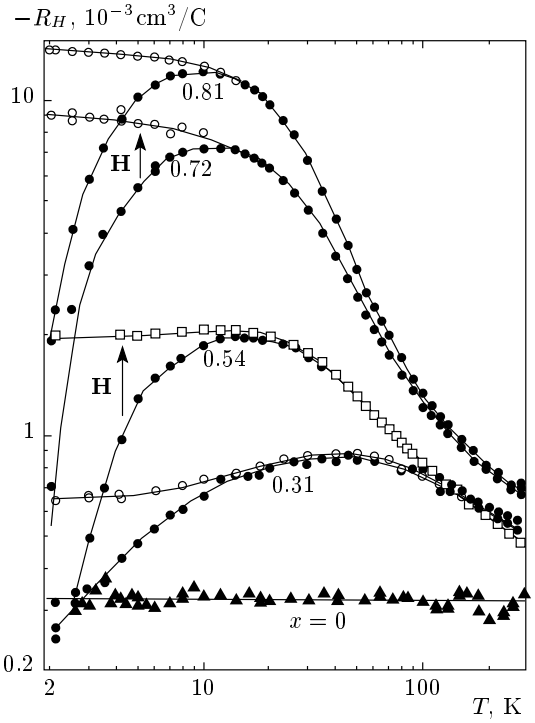

Fig. 10. Temperature dependences of the Hall coefficient $R_H(T, H_0) = \rho_{H1}(H, T)/H$ for solid solutions $Tm_{1-x}Yb_xB_{12}$ with $x = 0.31$, 0.54, 0.72, and 0.81 in magnetic fields $\mu_0 H = 1.5$, 7, and 8 T. The $R_H(T, H_0)$ dependence for the TmB_{12} ($x = 0$) compound in the magnetic field $\mu_0 H = 0.37$ T is shown for comparison

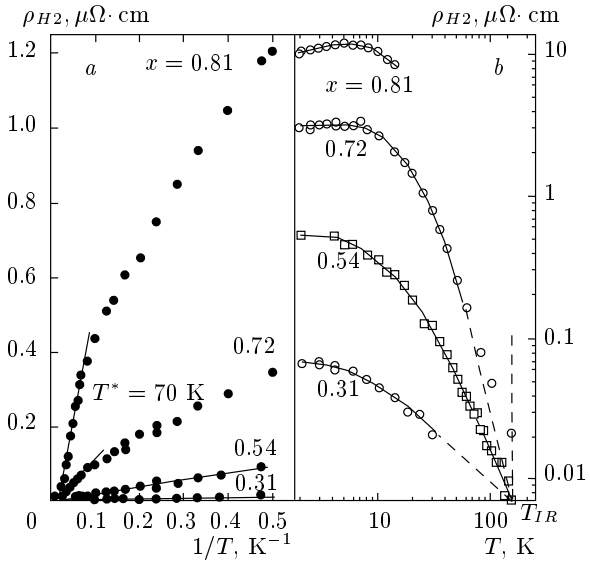

Fig. 11. Temperature dependences of the second-harmonic component $\rho_{H2}(H, T)$ in the Hall resistivity for (a) $\mu_0 H = 1.5$ T in the hyperbolic plot (see Eq. (10)) and (b) $\mu_0 H = 7$ (□) and 8 (○) T in the log–log scale

is certainly established here that the observed second harmonic term is a real TE effect and it is not an experimental artefact caused by the magnetoresistance contribution.

To study singular features of the Hall and transverse even effects in $Tm_{1-x}Yb_xB_{12}$ in a wide vicinity of the QCP and in the presence of the metal–insulator transition, we examined the angular dependences $\rho_H(\varphi)$ in detail for compounds with $x \approx 0.31 \approx x_c$ (QCP), $x \approx 0.54$, 0.72, and 0.81 at temperatures in the range 1.9–300 K and in magnetic fields up to 8 T. Furthermore, these main (odd) and even Hall resistivity contributions detected in accordance with relation (4) were analyzed quantitatively. Examples of the analysis of the $\rho_H(\varphi)$ curves are presented in Figs. 7*b–d* and 8*a–d*, where the decomposition of the experimental dependences into the main and even Hall resistivity components are shown for liquid-helium temperatures and various magnetic fields below $\mu_0 H = 8$ T (see dashed and dotted lines in Figs. 7 and 8). According to Figs. 7 and 8, relation (4) accurately describes the experimental data (solid lines in Figs. 7 and 8 are the sums of these two components in $\rho_H(\varphi)$) and allows both defining the amplitude values $\rho_{H1}(H, T)$ and $\rho_{H2}(H, T)$ for all compounds investigated and estimating the phase shift $\Delta\varphi(T, H)$ between the components in the signal from the Hall probes. Within the experimental accuracy, the phase shift serves as a constant $\Delta\varphi(T, H) \approx 15°$, whereas the amplitudes ρ_{H1} and ρ_{H2} for $Tm_{1-x}Yb_xB_{12}$ compounds vary considerably with the temperature and magnetic field. The temperature dependences of the Hall coefficient $R_H(H_0, T) = \rho_{H1}(H_0, T)/H$ and the second harmonic amplitude $\rho_{H2}(H_0, T) \equiv \rho_{TE}(H, T)$ are shown in Figs. 10 and 11. The magnetic field dependences of the Hall coefficient $R_H(T_0, H)$ and the even component $\rho_{H2}(T_0, H) \equiv \rho_{TE}(H, T)$ of the Hall resistivity obtained from the measurements at liquid-helium temperatures ($T_0 = 2.1$ and 4.2 K) for different ytterbium concentrations are presented in Figs. 12 and 13. For comparison, the results of the Hall coefficient measurements for TmB_{12} ($x = 0$) in the low magnetic field $\mu_0 H = 0.37$ T are also shown in Fig. 10.

3.3. Analysis of the contributions to the Hall resistivity

3.3.1. Hall coefficient

The usual contribution to the Hall effect (odd in magnetic field) increases drastically for Yb contents

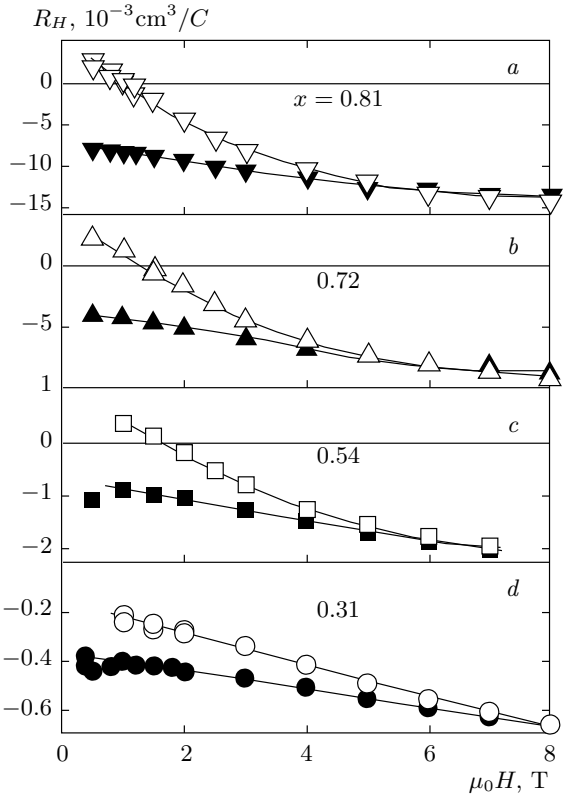

Fig. 12. Magnetic field dependences of the Hall coefficient $R_H(H)$ at liquid-helium temperatures $T_0 = 4.2$ K (closed symbols) and $T_0 = 2.1$ K (open symbols) for $Tm_{1-x}Yb_xB_{12}$ compounds with $x = 0.31$, 0.54, 0.72, and 0.81

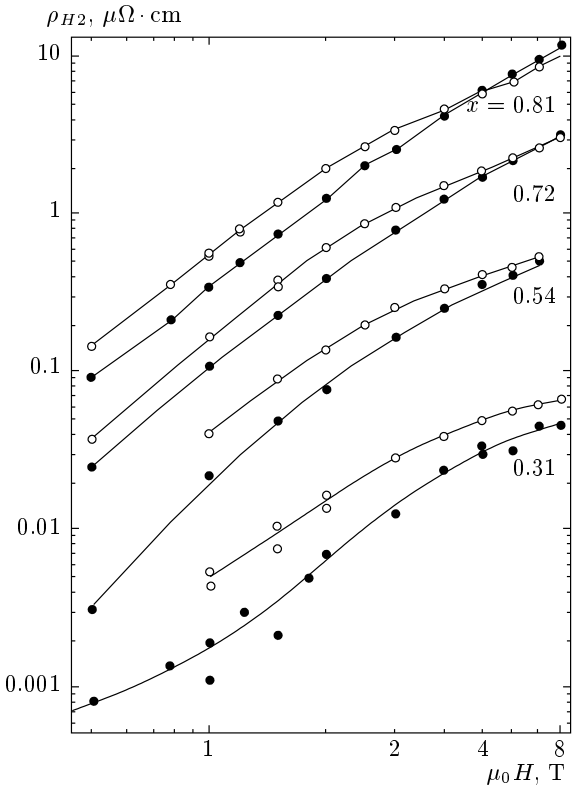

Fig. 13. Magnetic field dependences of the second-harmonic component $\rho_{H2}(H,T)$ in the Hall resistivity at liquid-helium temperatures $T_0 = 4.2$ K (closed symbols) and $T_0 = 2.1$ K (open symbols) for $Tm_{1-x}Yb_xB_{12}$ compounds with $x = 0.31$, 0.54, 0.72, and 0.81

above the quantum critical point ($x \geq x_c \approx 0.3$) with a decrease in the temperature in the range 30–300 K. Below 30 K, the amplitude of the negative Hall coefficient is strongly depressed and the sign reversal of $R_H(T)$ is observed at liquid-helium temperatures in the low magnetic field $\mu_0 H \leq 2$ T for samples with the Yb contents $x > x_c$ (Figs. 10 and 12). As a result, the Hall coefficient of the $Tm_{1-x}Yb_xB_{12}$ system with $x \geq x_c$ reveals a large-amplitude negative maximum at intermediate temperatures 10–50 K and, as x increases, the metal–insulator transition is accompanied by a shift of the remarkable feature of $R_H(T)$ downwards on the temperature scale together with a simultaneous increase in its amplitude.

A similar behavior of the opposite (positive) sign Hall coefficient with a maximum $R_H(T)$ at T_{max} and sign reversal at low temperatures was observed earlier for dense Ce- and U-based metallic heavy-fermion systems $CeAl_3$ [28], $CeCu_6$ [29], $CePd_3$ [30], UAl_2 [31], and UPt_3 [32] and for the so-called Kondo insulator CeNiSn [33]. The effect was attributed to the appearance of a many-body resonance at the Fermi energy E_F in the electron density of states and to a crossover to the coherent regime of the magnetic scattering of charge carriers in these strongly correlated electron systems. Moreover, using detailed Hall effect measurements of the archetypal heavy fermion compounds $CeAl_2$ [27], $CeAl_3$ [6, 34], $CeCu_6$ [6], and CeB_6 [35], a complicated activation-type dependence of the Hall coefficient,

$$R_H(T) \propto \exp(E_{a1,2}/k_B T), \qquad (5)$$

was certainly established in the temperature range $T > T_{max}$. It was noted previously [6, 27, 34, 35] that the activation-type behavior of $R_H(T)$ observed in these Ce-based metals is extremely unusual and cannot be explained in the framework of the Kondo lattice model or the model of skew scattering of charge carriers [36, 37]. In these models, the spin-flip resonant scattering of conduction electrons on the localized magnetic moments of rare earth ions is regarded as a

dominant factor determining the charge transport. In the approach developed in [36, 37], both the anomalous Hall effect and the nonmonotonic behavior of resistivity in heavy-fermion compounds should be exclusively attributed to the specific character of the scattering effects. At the same time, the spin-polaron approach, which is an alternative to the skew scattering model, treats the parameters $E_{a1,2}$ found for heavy-fermion Ce-based compounds as the binding energies of different type many-body states formed near Ce $4f$ centers [6, 27, 34, 35].

In the case of the Yb-based compounds under investigation, we recall that (i) Yb is a hole-type analogue of Ce and U in these strongly correlated electron systems and (ii) the metal–insulator transition occurs in the $Tm_{1-x}Yb_xB_{12}$ solid solutions. Therefore, the negative $R_H(T)$ extremum (see Fig. 10) should also be analyzed above the maximum at T_{max} in terms of Eq. (5). According to the activation plot in Fig. 14*a*, $R_H(T)$ curves for $Tm_{1-x}Yb_xB_{12}$ solid solutions with $x \geq 0.5$ can be well approximated by activation law (5) in the temperature intervals (I) 120–300 K and (II) 50–120 K. Furthermore, the energy gap $E_g \approx 200\ K \approx 17.8$ meV can be determined in range I. The value $E_g \approx 17.8$ meV estimated for $x = 0.54$, 0.72, and 0.81 (Fig. 14*a*) appears to be close to the gap found for the narrow-gap semiconductor YbB_{12} from the measurements of the Hall effect and resistivity ($E_g/k_B \approx 180$ and 134 K [13]), NMR on the Yb ions [14] and specific heat ($E_g/k_B \approx 170$ K [15]). It is also comparable to the spin gap value approximately 12 meV found in the inelastic neutron scattering [38, 39] and ESR [40] experiments.

Additionally, the activation-type dependence of the Seebeck coefficient in the intrinsic conductivity regime,

$$S = \frac{k_B}{e}\,\frac{b-1}{b+1}\,\frac{E_g}{2k_gT}, \qquad (6)$$

where $b = \mu_n/\mu_p$ is the electron-to-hole mobilities ratio and e is the electron charge, allows deducing the ratio $\mu_n/\mu_p \approx 7.7$ from the comparison of the slopes of the $S \propto 1/T$ [10] and $\ln|R_H| \propto 1/T$ dependences for $Tm_{1-x}Yb_xB_{12}$ solid solutions with $x \geq 0.5$ (Fig. 14*a*). We emphasize that the ratio $b = \mu_n/\mu_p \approx 50$ was previously obtained for another archetypal narrow-gap semiconductor, the intermediate valence compound SmB_6 [41]. The large b values in the regime of fast charge fluctuations were shown to be due to the low mobility μ_p of the heavy holes on the rare-earth ions compared to μ_n for conduction electrons in the $5d$ band.

In the spin-polaron approach, the parameters $E_g \equiv 2E_{a1}$ and $E_a \equiv E_{a2}$ in Eq. (5) obtained for $Tm_{1-x}Yb_xB_{12}$ with $x \geq 0.5$ can be treated as the binding energies of short-radius many-body states that are formed near Yb $4f$ centers in the matrix of these Yb-based dodecaborides. It is also worth noting that in the regime of charge transport via in-gap states (range II in Fig. 14*a*), the activation energy values E_a of the Hall (Fig. 14*a*) and Seebeck coefficients coincide with each other (see also [10]). In the spin-polaronic approach, the width of the quasielastic peak $\Gamma_0(T > 100\ \text{K})/2 \approx 12.5$ meV obtained from the neutron scattering experiments in YbB_{12} and $Yb_{1-x}Lu_xB_{12}$ solid solutions [16, 42] can be used in the simple relation

$$\Gamma_0(T > 100\ \text{K})/2 = \hbar/\tau_{eff}(T) \qquad (7)$$

in order to evaluate the relaxation time $\tau_{eff}(T \geq 100\ \text{K}) \approx 1.1 \cdot 10^{-13}$ s and, further on, to estimate the effective mass m^* of the heavy fermions from the Hall mobility $\mu_H(T) = R_H(T)/\rho(T)$ [6, 27, 34, 35]:

$$m^*(T) = e\tau_{eff}(T)/\mu_H(T). \qquad (8)$$

The temperature dependences of the Hall mobility for $Tm_{1-x}Yb_xB_{12}$ solid solutions deduced from the data in Figs. 5 and 10 are shown in Fig. 15. The calculated effective mass $m^*(T \approx 100\ \text{K}) \approx 24m_0$ for these Yb-based compounds is consistent with the values determined previously for the effective mass of the spin-polaron and exciton–polaron many-body states in the strongly correlated electron systems: $m^* \approx (20\text{–}90)m_0$ for FeSi [43], $m^* \approx (20\text{–}40)m_0$ for SmB_6 [41], $m^*_{1,2} \approx (55\text{–}90)m_0$ for $CeAl_2$ [27], $m^*_{1,2} \approx (45\text{–}90)m_0$ for $CeAl_3$ [34], $m^*_{1,2} \approx (130\text{–}150)m_0$ for $CeCu_6$ [6], and $m^* \approx 400m_0$ for CeB_6 [35]; it is also comparable with the estimate $m^* \approx (12\text{–}34)m_0$ obtained for YbB_{12} from optical measurements [44, 45] in the temperature range 20–200 K.

It is worth noting here that the most important mechanism that determines the mobility of charge carriers in the $Tm_{1-x}Yb_xB_{12}$ system is the scattering by on-site $4f$–$5d$ spin fluctuations. As a result, the carrier relaxation rates deduced from various experiments on YbB_{12} crystals [16, 42, 44, 45] and $Lu_{1-x}Yb_xB_{12}$ substitutional solid solutions [16, 42] at temperatures above 100 K are very close to each other. Moreover, the Hall mobilities obtained in the temperature range 100–200 K for $Tm_{1-x}Yb_xB_{12}$ single crystals with $x > 0.5$ in the presence of strong substitutional disorder (see Fig. 15) and for high-quality YbB_{12} samples (see [44, 45]) are roughly equal to each other (6–10 $\text{cm}^2/\text{V}\cdot\text{s}$) and have very similar temperature dependences. Hence, the estimate of the effective masses of heavy quasiparticles in $Tm_{1-x}Yb_xB_{12}$ using Eqs. (7)

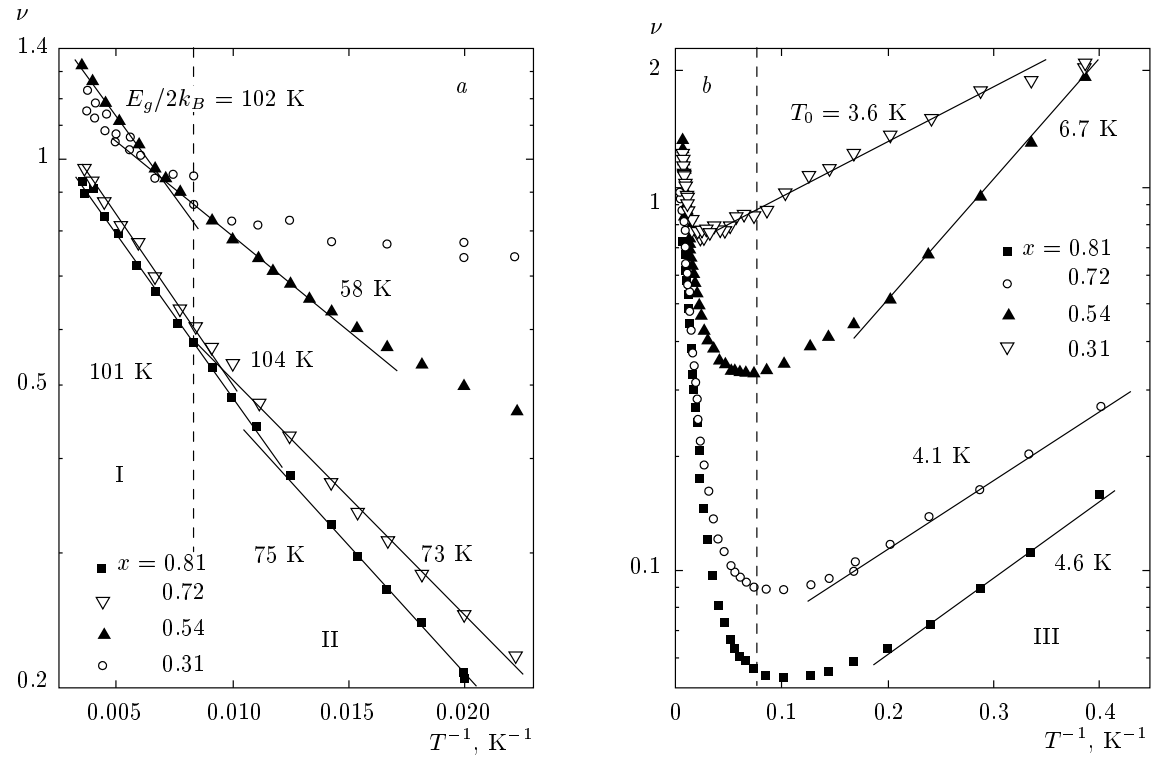

Fig. 14. Activation-type dependences of the reduced concentration $\nu = (R_H e N_{4f})^{-1}$ of charge carriers for $Tm_{1-x}Yb_xB_{12}$ compounds with $x = 0.31$, 0.54, 0.72, and 0.81 in the different temperature ranges I–III

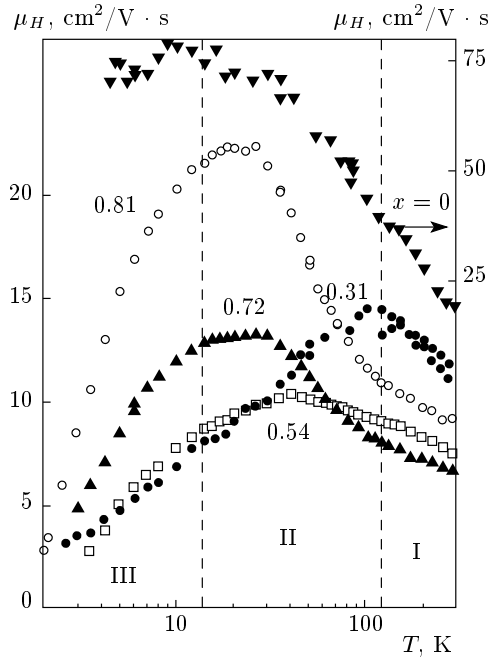

Fig. 15. Temperature dependences of the Hall mobility $\mu_H(T) = R_H(T)/\rho(T)$ in the series of $Tm_{1-x}Yb_xB_{12}$ compounds

and (8) and the neutron scattering results obtained in [16,42] for $Lu_{1-x}Yb_xB_{12}$ system is quite reasonable. With the known parameters E_a and E_g (Fig. 14*a*) and effective masses $m^*_{\mathrm{I,II}}$, using the relation

$$a_{p1,2} = \hbar/\sqrt{2E_{g,a}m^*_{\mathrm{I,II}}}, \qquad (9)$$

we can also estimate the localization radius of the many-body states. For these heavy fermions in the $Tm_{1-x}Yb_xB_{12}$ matrix in temperature intervals I (120–300 K) and II (50–120 K), this gives the respective values 5 and 9 Å. The same size about 5 Å of many-body exciton–polaron states was obtained in [44] from far-infrared quasioptical measurements of YbB_{12}. We note that in temperature range I of gap formation, the spatial extension of the complexes $a_{p1} \approx 5$ Å is approximately equal to the shortest distance (near 5.3 Å) between the R^{3+} rare-earth ions in the RB_{12} lattice; therefore, the many-body states are localized in the unit cell near rare-earth sites. As the temperature decreases in range II and approaches the coherent regime, the localization radius $a_{p2} \approx 9$ Å starts to exceed the lattice constant ($a \approx 7.5$ Å) and, moreover, the a_{p2} value increases simultaneously with the Yb concentration x when E_a varies in the interval 58–75 K (see

Fig. 14*a* and Eq. (9)). In this respect, it is natural to assume that a significant increase in the localization radius causes the formation of a filamentary structure of manybody states, resulting in a transition to the coherent state, which is displayed in the abrupt decrease in the Hall (see Fig. 10) and Seebeck [10] coefficients in $Tm_{1-x}Yb_xB_{12}$ solid solutions with strong electron correlations.

Another novel experimental result of this study was obtained at temperatures below the negative maximum of the Hall coefficient (range III, $T < T_{max}$, Figs. 14*b* and 15) in $Tm_{1-x}Yb_xB_{12}$ with $x > x_c$, where the temperature dependence of R_H has the form

$$R_H(T) \propto \exp(-T_0/T) \qquad (10)$$

with the estimated values $T_0 \approx 3.5$–7 K (Fig. 14*b*). A similar behavior of $R_H(T)$ was previously observed for heavy-fermion compounds $CeAl_2$ [27] and $CeAl_3$ [34] and was interpreted in terms of the dependence predicted in [46] for the Hall coefficient in a system with Berry phase effects, where the carrier moves by hopping in a topologically nontrivial spin background. According to [46, 47], the Hall effect is modified in such a situation because of the appearance of the internal magnetic field $H_{int} = \langle h_z \rangle \sim (1/k_BT)\exp(-T_0/T)$, which is added to the external field H.

When inducing the polarization of both the localized magnetic moments of rare earth ions and the spins of conduction electrons, the external magnetic field suppresses the coherence in the spin-flip scattering in the periodic system of rare earth centers. As a result, the sign reversal of $R_H(H, T_0)$ is observed in the magnetic field at liquid-helium temperatures (see the curves in Fig. 12 for $Tm_{1-x}Yb_xB_{12}$ with $x = 0.54$, 0.72, and 0.81 at $T_0 = 2.1$ K). Moreover, the Hall coefficient $R_H(T)$ appears to be nearly temperature independent in strong magnetic fields (see Fig. 10). We note that the Hall coefficient behavior in the magnetic field in $Tm_{1-x}Yb_xB_{12}$ is quite different from that reported previously for archetypal Ce- and U-based heavy fermion systems [6, 27–34] and observed in HoB_{12} [48]. Indeed, in the abovementioned compounds, the depression of the Hall effect amplitude is usually observed in high magnetic fields. Moreover, the $R_H(H)$ decrease is much more pronounced at temperatures below the Hall coefficient maximum in the interval $T < T_{max}$. The opposite trend of the Hall effect enhancement in the magnetic field established here (see Fig. 10 for $Tm_{1-x}Yb_xB_{12}$ compounds under investigation) is similar to the effect observed recently for rare-earth hexaborides $Ce_{1-x}La_xB_6$ [49], PrB_6 and NdB_6 [50, 51], and it was attributed to the magnetization of spin-polaron many-body states by the external magnetic field.

To conclude this section, we roughly estimate the localization radius of the many-body states in another way, from the results in Fig. 14*b*. The decrease in the reduced concentration of charge carriers per rare-earth ion $\nu = (R_H e N_{4f})^{-1}$ (where $N_{4f} = 0.96 \cdot 10^{22}$ cm^{-3} is the concentration of rare-earth ions in RB_{12}, R–Tm, and Yb) in the interval $0.08 < \nu \leq 0.8$ can be treated as an increase in the effective volume per conduction electron, which we attribute to the formation of many-body states in $Tm_{1-x}Yb_xB_{12}$. Taking the R^{3+}–R^{3+} distance (about 5.3 Å) in the fcc crystal structure of the dodecaboride compounds under investigation into account, we obtain the crude estimate $a_{p2} = 6$–12 Å for temperatures near the negative $R_H(T)$ maximum for the solid solutions with the Yb content in the range $x \geq x_c$. It is worth noting that the deduced a_{p2} values agree very well with the aforementioned results based on Eq. (9).

3.3.2. Second harmonic contribution to the Hall resistivity (TE effect)

When analyzing the even Hall resistivity component, it is worth noting that the discussion of quadratic contributions to the Hall effect can be found in early articles by Kohler (1934) and by Shoenberg (1935) (see [52] and the references therein). The TE effect was previously observed in studies of gallium [53] and n-type germanium [54]. Numerous examples of experimental observation of the transverse even effect are attributed to the case of induced anisotropy in a normally isotropic conductor, and their theoretical justification was given in [26]. Among them, well-known examples of the TE effect are provided by (i) mono- and polycrystalline ferromagnets, where the induced anisotropy is made evident through saturation, and (ii) the nonmagnetic cubic metals having an induced anisotropic conductivity in the high-field condition because of the operation of open orbits [26]. On the other hand, for the normal state of high-T_c superconductors (HTSCs), in addition to the crystalline anisotropy, the origin of the transverse even effect is usually attributed to the appearance of stripes on the surface and in HTSC layers [55].

When analyzing the second-harmonic component in ρ_H — the TE effect in the $Tm_{1-x}Yb_xB_{12}$ system — it is worth noting that the contribution of this kind has been found earlier in the strongly correlated antiferromagnets $CeAl_2$[27], CeB_6 [35, 56, 57], PrB_6 [50], NdB_6 [50, 51], and ErB_{12} [18] both in the paramag-

netic and magnetically ordered phases. An even harmonic $\rho_H \propto \cos 2\varphi$ in the angular dependences of the Hall signal was also observed in the narrow-gap semiconductor FeSi [43, 58] in a wide range of temperatures near the mictomagnetic (spin-glass) phase transition. A detailed study of the second-harmonic term was performed recently for $CeCu_{6-x}Au_x$ solid solutions [6, 59], where the Hall and TE effect anomalies were investigated in the vicinity of the AF quantum critical point $x_c \approx 0.1$. It was certainly established that the development of the antiferromagnetic instability in these model compounds is accompanied by both a remarkable increase in the low-temperature Hall coefficient $R_H(x)$ at $x \approx x_c$ and the appearance of the even-harmonic contribution $\rho_{H2}(x, T, H)$ whose amplitude is maximal at the QCP [6]. Moreover, for the series of compounds $CeCu_{6-x}Au_x$ in the concentration range $0 \le x \le 0.15$, the temperature dependences $\rho_{H2}(T)$ near the QCP are approximated with a high accuracy by a hyperbolic dependence of the form

$$\rho_{H2}(T) \approx C^*(1/T - 1/T^*). \qquad (11)$$

The hyperbolic divergence of the Hall resistivity component $\rho_{H2}(T)$ was established to be the singular feature of the regime of quantum critical behavior, together with other anomalies including the logarithmic divergence of the electron term in the heat capacity $C(T)/T \propto \ln T$, non-Fermi-liquid behavior of the resistivity $\rho(T) \propto T$, power-law asymptotic behavior of the magnetic susceptibility $\chi(T) \propto T^{-\beta}$, and so on [60–70], which are associated with the divergence of the effective mass of many-body states (heavy fermions) near the QCP.

The second-harmonic contribution to the Hall signal ρ_H of $Tm_{1-x}Yb_xB_{12}$ solid solutions detected in this study (see Fig. 11*a*) was analyzed in magnetic fields below 2 T in terms of Eq. (11). It was found that the $\rho_{H2}(T)$ evidently follows the hyperbolic dependence given by Eq. (11) with the characteristic temperature $T^* \approx 70$ K, which is common for any Yb contents in the range $x \ge x_c$. The slope $C^*(x)$ of the hyperbolic dependence increases dramatically (by more than an order of magnitude) when the metal–insulator transition occurs in the series of $Tm_{1-x}Yb_xB_{12}$ compounds, and the tendency to saturation of the $\rho_{H2}(1/T)$ curve is observed at temperatures below 10 K only for the highest Yb composition (Fig. 11*a*). Additionally, the amplitude $\rho_{H2}(T_0, H)$ of this transverse even effect at liquid-helium temperatures increases by more than two orders of magnitude in external magnetic fields up to 8 T (see Fig. 13). The log–log plot of the Hall resistivity temperature dependence $\rho_{H2}(T, H_0)$ is shown in Fig. 11*b*

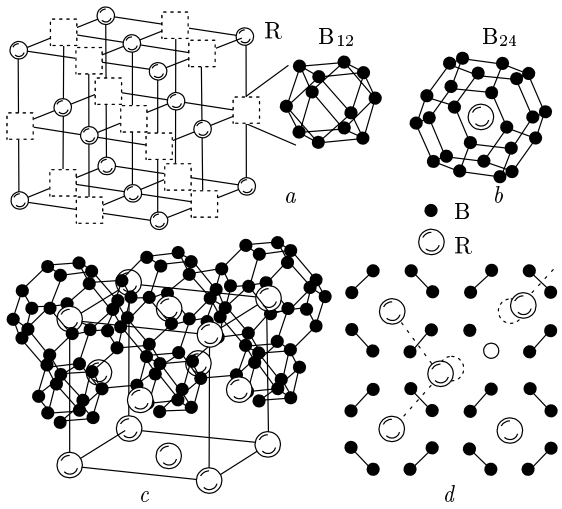

Fig. 16. (*a*) Crystal structure of $Tm_{1-x}Yb_xB_{12}$ compounds. The NaCl-type unit cell is built from R^{3+} ions and B_{12} cubooctahedrons. (*b*) The first coordination sphere of R^{3+} is arranged as a truncated octahedron B_{24}. The arrangement of R and B atoms along the direction $\langle 110 \rangle$ and in the (110) section is presented in (*c*) and (*d*), respectively. For clarity, B_{12} and B_{24} clusters are shown in (*c*) only along the upper face diagonal of the lattice. The lattice defect (boron vacancy) is shown (small open circle) in the (110) section (*d*). The broken R–B bonds in the vicinity of the boron vacancy cause displacements of the nearest R^{3+} ions away from the defect on 0.4 Å distance along $\langle 100 \rangle$ [25]. As a result of random displacements of the R^{3+} ions, the R^{3+} dimers and other small-size rare earth clusters (shown in view (*d*) for convenience) appear in the RB_{12} matrix

for the highest magnetic fields $\mu_0 H_0 = 7$–8 T used in the study. In the high magnetic fields, the second-harmonic contribution appears at $T_{IR} \approx 130$–150 K, increases drastically with a decrease in the temperature, and saturates at liquid-helium temperatures for all the Yb concentrations $x \ge x_c$ (Fig. 11*b*).

At the end of this section, we summarize both a significant difference and similarities in the behavior of the second-harmonic contribution near the AF QCP in the heavy-fermion systems with metal conductivity and in compounds with the metal–insulator transition. In the heavy-fermion metals $CeCu_{6-x}Au_x$, the TE anomalous contribution is observed in a narrow region close to the AF QCP [6], whereas in the second-type systems with the metal–insulator transition, the $\rho_{H2}(H, T) \equiv \rho_{TE}(T_0, H)$ component appears near the QCP at $x = x_c \approx 0.3$ and its amplitude increases dramatically with x when the metal–insulator transition occurs (see Figs. 11 and 13). At the same time,

in both the metallic and dielectric systems with the AF QCP, the characteristic temperature T^* in hyperbolic relation (11) is positive (see Fig. 11*a* and [6]) and, in our opinion, T^* values can probably be associated with the appearance of structural distortions and disordering in these compounds. Indeed, the order–disorder phase transition at $T^* \approx 60$–70 K was found very recently in the reference nonmagnetic dodecaboride compound LuB_{12} [24]. Moreover, a comprehensive study of the heat capacity and Raman scattering spectra in the Lu^NB_{12} crystals with various boron isotope concentrations (N = 10, 11, and natural) allowed the authors of Ref. [25] to conclude in favor of the cage-glass type phase transition at T^* in the family of rare-earth dodecaborides RB_{12}. In addition, it was shown in [25] that the combination of the loosely bound state of the rare-earth ions in the rigid boron sublattice of RB_{12} compounds (see also Fig. 16*a*–*c*) together with the randomly arranged boron vacancies provokes the development of vibrational instability at intermediate temperatures and the Ioffe–Regel limit is reached in the RB_{12} family at $T_{IR} \approx 130$–150 K. As a result, the anomalies at 150 K in both the μSR spectra [71, 72] and high-resolution photoemission spectroscopy [73] data together with the Hall mobility features at $T_{IR} \approx 130$–150 K (see Fig. 15) may be attributed to the crossover from the phonon-assisted regime to the regime of quasilocal vibrations in the scattering of charge carriers.

We emphasize that when comparing the metallic and dielectric systems with the antiferromagnetic QCP, similarly to the structural changes in $Tm_{1-x}Yb_xB_{12}$ at T^*, the transition from the orthorhombic to monoclinic structure in the QCP solid solution $CeCu_{5.9}Au_{0.1}$ was evidently established at $T_S \approx 70$ K [74, 75], and it was shown that the transformation is accompanied by slight distortions of the bond angles. Because the quantum critical regime is suppressed by the external magnetic field, a natural explanation for the magnetic field dependences $\rho_{H2}(H)$ may be found. Indeed, in systems of both types, a sharp increase in $\rho_{H2}(H)$ in the range $\mu_0 H \leq 3$ T is accompanied by the destruction of the hyperbolic temperature dependence (Eq. (11)) and, as a result, the quantum critical regime falls down and the tendency to the saturation of $\rho_{H2}(H)$ is observed in magnetic fields above 5 T.

3.3.3. Quantum critical point and the metal–insulator transition

When discussing the renormalization effects in the density of states at the metal–insulator transition in the series of $Tm_{1-x}Yb_xB_{12}$ compounds, it is interesting to begin with the properties of the TmB_{12} metal. An almost temperature-independent behavior of the Hall coefficient was detected for this compound in magnetic fields up to 8 T (see, e. g., the curve for $\mu_0 H = 0.37$ T in Fig. 10). The value $R_H(T) \approx$ const $\approx -3.25 \cdot 10^{-4}$ cm^3/C in the approximation of one group of charge carriers is roughly equal to the reduced carrier concentration per rare-earth ion $\nu = (R_H e N_{4f})^{-1} \approx 2$. Hence, TmB_{12} appears to nearly correspond to the case of a two-electron metal. Above the Néel temperature $T_N \approx 3.2$ K, the resistivity of TmB_{12} exhibits a minimum at 11 K and a maximum at 6.5 K [76]. Moreover, a remarkable negative magnetoresistance [76] and positive contribution to the Seebeck coefficient [18] at temperatures below 40 K were found. The authors of [18, 76] concluded in favor of strong local $4f$–$5d$ spin fluctuations and the spin-polaron approach was applied to explain the properties of this rare earth dodecaboride.

The Tm-to-Yb substitution in the range $x \leq x_c \approx 0.3$ is accompanied by the development of the AF instability in the $Tm_{1-x}Yb_xB_{12}$ family, resulting in a gradual T_N decrease (Fig. 17*a*, where the range $0 \leq x \leq 1$ corresponds to the filling of the $4f$ shell in the interval $12 \leq n_{4f} \leq 13$ in the $Tm_{1-x}Yb_xB_{12}$ solid solutions, and $n_{4f} = 10$, 11, and 14 respectively correspond to HoB_{12}, ErB_{12}, and LuB_{12}). The extrapolation of the $T_N(x)$ dependence to the value $T_N = 0$ gives $x_c \approx 0.3$ in the series of $Tm_{1-x}Yb_xB_{12}$ solid solutions (QCP in Fig. 17*a*). The quantum critical behavior was probably observed in $Tm_{0.74}Yb_{0.26}B_{12}$ for the magnetic contribution to the specific heat with a logarithmic divergence of the form $C/T \propto \ln T$ at $T < 4$ K [77]. At the same time, the complicated activation-type behavior of the Seebeck coefficient $S(T)$ (see Eq. (6)) was found in [10] at intermediate temperatures (intervals I and II) for all $Tm_{1-x}Yb_xB_{12}$ compounds with $x \geq 0.05$. Moreover, for AF compounds with the Yb content $0.05 \leq x < x_c \sim 0.3$, both the gap formation in range I (120–300 K) and the charge transport regime through the many-body intra-gap states with the binding energy E_a (interval II, 50–120 K) are detected on the $S(T)$ dependences simultaneously with the weak localization features of the resistivity (see Fig. 5) and a moderate increase in the Hall coefficient (Figs. 10 and 14*a*). In the paramagnetic state just above the QCP $x_c \approx 0.3$, the increase in the Yb concentration induces a remarkable increase in the Hall coefficient $R_H(x)$ together with the appearance and a drastic increase in the second-harmonic component $\rho_{H2}(x)$ (the TE effect) in the Hall resistivity (Fig. 17*b*). Furthermore, in view of

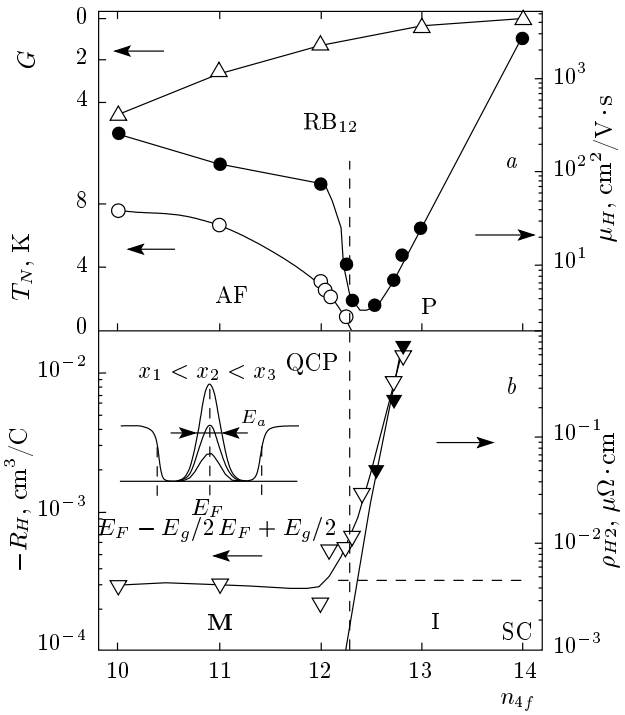

Fig. 17. (a) The de Gennes factor $G = (g_J - 1)^2 \times \times J(J+1)$, the Hall mobility $\mu_H(n_{4f})$ at liquid-helium temperature (the data for HoB_{12} ($n_{4f} = 10$), ErB_{12} ($n_{4f} = 11$), and LuB_{12} ($n_{4f} = 14$) are taken from [18, 56] and the data for YbB_{12} ($n_{4f} \approx 13.05$) are taken from [44, 45]) and the Néel temperature $T_N(n_{4f})$ versus the filling of the $4f$ shell of the rare-earth ions in the RB_{12} compounds; AF and P denote the antiferromagnetic and paramagnetic phases; M, I, and SC mean the metal, insulator, and superconductor, and QCP is the quantum critical point. (b) The Hall coefficient $R_H(n_{4f})$ and even-harmonic contribution $\rho_{H2}(n_{4f})$ for $\mu_0 H = 1.5$ and 8 T. The inset shows the renormalization effect in the density of states in the series of $Tm_{1-x}Yb_xB_{12}$ compounds

the activation-type behavior of $R_H(T)$ for $x > 0.5$, the gap value $E_g \approx 17.8$ meV and the width $E_a/k_B \approx 58$–75 K of the intra-gap many-body resonance on E_F (see the inset in Fig. 17b) can be obtained from the temperature dependence of the reduced carrier concentration (see Fig. 14a), and, finally, the effective mass $m^*(T \approx 100\ \text{K}) \approx 24m_0$ and localization radii of these many-body states $a^*_{p1} \approx 5$ Å (range I, 120–300 K) and $a^*_{p2} \approx 9$ Å(range II, 50–120 K) are estimated. Since the spatial extension of the complexes $a^*_{p1} \approx 5$ Å is roughly equal to the shortest distance (5.3 Å) between the R^{3+} ions in the RB_{12} lattice, this provides strong evidence in favor of the conclusion made in [25] concerning the formation of R^{3+}–R^{3+} dimers and the appearance of short range rare-earth-based vibration clusters in the matrix of the dodecaboride compounds. Figures 16 illustrate the mechanism of an emergence in the RB_{12} matrix of the nanosize clusters arranged from the R^{3+} ions in the presence of randomly distributed boron vacancies. A similar conclusion was made in [78], where the existence of Yb–Yb pairs was deduced from the results of electron spin resonance experiments in the narrow-gap semiconductor YbB_{12}. Moreover, the dipole–dipole splitting of the resonance lines permitted the estimate $r_{p2} = 9.1$ Å [78] for the distance between the interacting ytterbium pairs in YbB_{12}, which is roughly equal to the a_{p2} value obtained above for $Tm_{1-x}Yb_xB_{12}$ compounds.

Taking into account that the localization radius of the intra-gap states $a^*_{p2} \approx 8$–9 Å in range II exceeds the lattice constant ($a \approx 7.5$ Å) and the size increases with the Yb concentration x in the $Tm_{1-x}Yb_xB_{12}$ series, the coherent regime of charge transport may be attributed to the percolation through the network of many-body states in the RB_{12} matrix. From this standpoint, a quite natural interpretation may be suggested to explain the origin of the unusual dependence given by Eq. (10) for the Hall coefficient behavior in the coherent state. Indeed, at helium temperatures and for $x \geq 0.5$ on the metallic side of the percolation limit (coherent regime), the magnetic system of the intra-gap many-body states, which is a filamentary structure arranged on the small magnetic clusters of rare-earth ions, should be regarded as a system with a topologically nontrivial configuration of the core spins. As a result, the appearance of the Berry phase effect produces the internal magnetic field

$$H_{int} = \langle h_z \rangle \sim \frac{1}{k_B T} \exp\left(-\frac{T_0}{T}\right)$$

and the Hall coefficient is modified in agreement with the prediction made in [46, 47]. It is also worth noting that simultaneously with a drastic decrease in the Hall coefficient, which is accompanied by the sign reversal of $R_H(T)$ observed at low temperatures in the coherent regime (interval III), a nearly linear temperature dependence of the Seebeck coefficient was established for $Tm_{1-x}Yb_xB_{12}$ solid solutions at temperatures $T < 30$ K [10]. A variation of the slope of the Mott-type diffusive thermopower $S(T)$ in the metallic coherent state allowed the authors of Ref. [10] to estimate the order of magnitude of the renormalization effect in the density of states near the Fermi energy E_F when the many-body resonance appears with an increase in x in the series of $Tm_{1-x}Yb_xB_{12}$ solid solutions (see also the inset in Fig. 17b).

We emphasize that the local on-site $4f$–$5d$ spin fluctuations play the dominant role in the charge transport in $Tm_{1-x}Yb_xB_{12}$ dodecaborides. Indeed, when n_{4f} increases from HoB_{12} to LuB_{12} in the range $10 \le n_{4f} \le 14$, we should expect a monotonic increase in $\mu_H(n_{4f})$, which follows from a decrease in the de Gennes factor $(g_J-1)^2J(J+1)$ characterizing the magnetic scattering intensity in the RB_{12} series. Instead, below the QCP in the range $10 \le n_{4f} \le 12.3$, a decrease in $\mu_H(n_{4f})$ is observed (Fig. 17*a*), and the mobility minimum near $x = 0.3$–0.5 in $Tm_{1-x}Yb_xB_{12}$ corresponds to the antiferromagnetic–paramagnetic transition with the QCP near $x_c \approx 0.3$. Furthermore, the substitution of Yb for Tm in the range $x \ge 0.5$ ($n_{4f} \ge 12.5$ in Fig. 17*a*) leads to an increase in $\mu_H(x)$, while a monotonic and sharp increase in the resistivity $\rho(x)$ (Fig. 5) and the Hall coefficient $R_H(x)$ (Fig. 17*b*) at low temperatures is observed in the range $0 < x < 1$ (the values of $\rho(T)$ and $R_H(T)$ in semiconductor YbB_{12} reach 10 $\Omega \cdot$ cm and 88 cm^3/C [13, 79, 80]). The metal–insulator transition is accompanied by rather low mobility values $\mu_H(T) \approx 27$ $cm^2/V{\cdot}s$ in YbB_{12}, which are obviously caused by the scattering of carriers on strong spin and charge $4f$–$5d$ fluctuations. Then, in passing to the nonmagnetic superconducting metal LuB_{12} ($n_{4f} = 14$), the Hall mobility increases drastically ($\sim$ 100 times) to $\mu_H \approx 2600$ $cm^2/V{\cdot}s$ (see Fig. 17*a*).

When comparing the metallic heavy-fermion compounds with quantum critical behavior, on the one hand, and $Tm_{1-x}Yb_xB_{12}$ solid solutions having the AF QCP and metal–insulator transition, on the other, it is worth mentioning the inelastic neutron scattering results obtained in [64, 81] for $CeCu_{5.9}Au_{0.1}$ and in [39] for YbB_{12}. The authors of Refs. [64, 81] concluded that the dimension of the magnetic excitation spectrum decreases near the QCP in $CeCu_{5.9}Au_{0.1}$ and its features coincide with the magnetic reflections detected in the AF state of antiferromagnets $CeCu_{5.8}Au_{0.2}$ and $CeCu_{5.7}Au_{0.3}$. A similar quasi-two-dimensional ($2D$) character of the spin fluctuation spectrum was revealed in [39] for YbB_{12}. Indeed, the M1 peak in the magnetic excitation spectrum of YbB_{12} was attributed to AF correlations at the wave vector (1/2 1/2 1/2). Assuming that the intensity distribution reflects the range of AF interactions between the Yb moments, the authors of [39] estimated correlation lengths perpendicular and parallel to the above direction, respectively corresponding to couplings within ($\xi_\parallel$) and between ($\xi_\perp$) the (001) planes. The values $\xi_\parallel = (5.4 \pm 1.4)$ Å and $\xi_\perp = (3.4 \pm 1.1)$ Å obtained in [39] confirm the $2D$ anisotropy. Moreover, we believe that this allows supposing the formation of some network of many-body states with the most effective interaction between Yb–Yb pairs in YbB_{12}.

These $2D$ effects in $CeCu_{5.9}Au_{0.1}$ were interpreted in [6] in terms of both local on-site $4f$–$5d$ fluctuations arising from the instability of the rare-earth ion configuration and long-wavelength fluctuations due to the development of the AF instability in the vicinity of the quantum phase transition. According to the approach developed in [6], fast local $4f$–$5d$ spin fluctuations lead to a renormalization of the effective mass of charge carriers via the formation of spin polarons (resonance at E_F) in heavy-fermion paramagnets. The appearance of long-wavelength fluctuations near the QCP at $T_N = 0$ in addition to the on-site ones is equivalent to "switching on" the interaction between the spin-polaron complexes, leading to the formation of a network of interconnected heavy-fermion states. As a result, the character of the quasiparticle interactions changes abruptly at the QCP (non-Fermi-liquid behavior) [67–70], and new anomalous features (the reduction of the dimensionality of the spin fluctuations [63, 64], unusual scaling of the dynamic magnetic susceptibility [7, 8], and so on) are observed. In our opinion, the same mechanism is responsible for the formation of a network of many-body states in the matrix of Tm_{1-x} Yb_xB_{12} solid solutions. However, in this case, when passing from the metal with strong $4f$–$5d$ spin fluctuations (TmB_{12}) to the intermediate valence narrow-gap semiconductor (YbB_{12}), the local on-site fluctuations increase dramatically, and in addition to the AF QCP at $x_c \approx 0.3$ (AF instability), both the continuous metal–insulator transition (Fig. 17*b*) and the vibration instability are developed with the formation of a cage-glass state at temperatures below $T^* \approx 70$ K [25]. In our opinion, the huge transverse even effect $\rho_{TE} \equiv \rho_{H2}$ observed in this study, which appears at x_c and increases drastically above the QCP (Fig. 17*b*), is also due to the formation of a structure of interconnected spin-polaron states in the conduction band of the $Tm_{1-x}Yb_xB_{12}$ compounds. At the same time, the theoretical description of the TE effect observed in the vicinity of a QCP is still an open question, and the results of present experimental study therefore provide the necessary background for understanding this phenomenon.

4. CONCLUSIONS

The detailed measurements of the resistivity in the Hall geometry including Hall and transverse even effects in substitutional solid solutions $Tm_{1-x}Yb_xB_{12}$

with $x \leq 0.81$ allow separating and classifying various contributions to charge transport in these strongly correlated electron systems. The comprehensive analysis of the angular, temperature, and field dependences of the Hall probes' resistivity has been carried out for these compounds close to the antiferromagnet–paramagnet and metal–insulator transitions in a wide vicinity of the QCP at $x_c \approx 0.3$ at temperatures 1.9–300 K in magnetic fields up to 8 T. It was found for the first time that the second-harmonic contribution (TE effect) appears in the angular dependences of the Hall probe's resistivity of the $Tm_{1-x}Yb_xB_{12}$ dodecaborides near the QCP, and it enhances as the concentration x increases in the interval $x \geq x_c$. A pronounced negative maximum on the temperature dependence of the Hall coefficient for $x \geq x_c$ and sign reversal of $R_H(T)$ at liquid-helium temperatures for $Tm_{1-x}Yb_xB_{12}$ compounds with $x \geq 0.5$ have been revealed and a decrease in $R_H(T)$ at $T < 30$ K has been identified as a singular feature of the coherent regime of charge transport. It has been shown that the external magnetic field drastically enforces the TE effect, also suppressing the coherent regime of the spin-flip scattering of charge carriers on the magnetic moments of rare-earth ions. For the $Tm_{1-x}Yb_xB_{12}$ compounds with $x \geq 0.5$ in the intervals 120–300 K and 50–120 K, we have found an activation-type dependence of the Hall coefficient with the activation energies $E_g \approx 17.8$ meV and $E_a/k_B \approx 58$–75 K and the following microscopic parameters: effective masses $m^* \approx 20m_0$ and localization radii of the heavy-fermion many-body states $a^*_{p1} \approx 5$ Å (120–300 K) and $a^*_{p2} \approx 9$ Å (50–120 K). It is argued in this study that the metal–insulator transition, which develops both in YbB_{12} as the temperature decreases and in $Tm_{1-x}Yb_xB_{12}$ solid solutions as the Yb concentration increases in the range $0 < x \leq 1$, is induced by a formation of Yb^{3+} dimers randomly distributed in the RB_{12} matrix. In the framework of the spin-polaron approach, the appearance of the aforementioned odd $R_H(T,H)$ and even $\rho_{TE}(T,H) \equiv \rho_{H2}(T,H)$ anomalous components in the resistivity detected in the Hall effect geometry in the $Tm_{1-x}Yb_xB_{12}$ series has been discussed in terms of the interference effects between local $4f$–$5d$ and long-range spin fluctuations, leading to the formation of a filamentary structure (network) of the interconnected many-body complexes in the dielectric matrix of these compounds.

We are grateful to G. E. Grechnev, A. V. Kuznetsov, V. V. Moshchalkov, D. A. Parshin, and J. Stankiewicz for the stimulating discussions. This work was supported by the Division of Physical Sciences, Russian Academy of Sciences (the Program "Strongly Correlated Electrons in Metals, Semiconductors, and Magnetic Materials"), the RFBR (grant No. 10-02-00998-a), and the Russian State Program "Human Resources of Innovative Russia". N. E. S., A. V. B., and V. V. G. are grateful to the Institute for Nanoscale Physics and Chemistry, of Katholieke Universiteit Leuven for the hospitality and support during their research visits.

REFERENCES

1. P. Coleman, C. Pepin, Q. Si, and R. Ramazashvili, J. Phys.: Condens. Matter **13**, R723 (2001).
2. P. Coleman, J. B. Marston, and A. J. Schofield, Phys. Rev. B **72**, 245111 (2005).
3. S. Paschen, T. Luhmann, S. Wirth et al., Nature **432**, 881 (2004).
4. A. Yeh, Yeong-Ah Soh, J. Brooke et al., Nature **419**, 459 (2002).
5. M. R. Norman, Q. Si, Ya. B. Bazalij, and R. Ramazashvili, Phys. Rev. Lett. **90**, 116601 (2003).
6. N. E. Sluchanko, D. N. Sluchanko, N. A. Samarin et al., Low Temp. Phys. **35**, 544 (2009).
7. A. Schroder, G. Aeppli, R. Coldea et al., Nature **407**, 351 (2000).
8. Q. Si, S. Rabello, K. Ingersent, and J. L. Smith, Nature **413**, 804 (2001).
9. Q. Si, S. Rabello, K. Ingersent, and J. L. Smith, Phys. Rev. B **68**, 115103 (2003).
10. N. E. Sluchanko, A. V. Bogach, V. V. Glushkov et al., Pis'ma v Zh. Eksp. Teor. Fiz. **89**, 298 (2009).
11. A. Czopnik, A. Murasik, L. Keller et al., Phys. Stat. Sol. (b) **221**, R7 (2000).
12. K. Siemensmeyer, K. Flachbart, S. Gabani et al., J. Sol. St. Chem. **179**, 2748 (2006).
13. F. Iga, N. Shimizu, and T. Takabatake, J. Magn. Magn. Mater. **177–181**, 337 (1998).
14. K. Ikushima, Y. Kato, M. Takigawa et al., Physica B **281–282**, 274 (2000).
15. F. Iga, S. Hiura, J. Klijn et al., Physica B **259–261**, 312 (1999).
16. P. A. Alekseev, E. V. Nefedova, U. Staub et al., Phys. Rev. B **63**, 064411 (2001).

17. V. Pluzhnikov, N. Shitsevalova, A. Dukhnenko et al., J. Magn. Magn. Mater. **320**, 1597 (2008).

18. N. Sluchanko, L. Bogomolov, V. Glushkov et al., Phys. St. Sol. (b) **243**, R63 (2006).

19. H. Okamura, S. Kimura, H. Shinozaki et al., Phys. Rev. B **58**, R7496 (1998).

20. V. N. Antonov, B. N. Harmon, and A. N. Yaresko, Phys. Rev. B **66**, 165209 (2002).

21. M. Heinecke, K. Winzer, J. Noffke et al., Z. Phys. B **98**, 231 (1995).

22. N. Okuda, T. Suzuki, I. Ishii et al., Physica B **281–282**, 756 (2000).

23. B. Jäger, S. Paluch, O. J. Żogał et al., J. Phys.: Condens. Matter **18**, 2525 (2006).

24. N. E. Sluchanko, A. N. Azarevich, A. V. Bogach et al., Zh. Eksp. Teor. Fiz. **138**, 315 (2010) [J. Exp. Theor. Phys. **111**, 279 (2010)].

25. N. E. Sluchanko, A. N. Azarevich, A. V. Bogach et al., Zh. Eksp. Teor. Fiz. **140**, 536 (2011) [J. Exp. Theor. Phys. **113**, 468 (2011)].

26. C. M. Hurd, Adv. Phys. **23**, 315 (1974).

27. N. E. Sluchanko, A. V. Bogach, V. V. Glushkov et al., Zh. Eksp. Teor. Fiz. **125**, 906 (2004).

28. F. G. Aliev, N. B. Brandt, G. S. Burkhanov et al., Pis'ma v Zh. Eksp. Teor. Fiz. **43**, 674 (1986).

29. T. Penney, F. P. Milliken, S. von Molnar et al., Phys. Rev. B **34**, 5959 (1986).

30. A. Fert, P. Pureur, A. Hamzic, and J. P. Kappler, Phys. Rev. B **32**, 7003 (1985).

31. M. Hadzic-Leroux, A. Hamzic, A. Fert et al., Europhys. Lett. **1**, 579 (1986).

32. A. Hamzic and A. Fert, J. Magn. Magn. Mater. **76/77**, 221 (1988).

33. T. Takabatake, M. Nagazawa, H. Fujii et al., J. Magn. Magn. Mater. **108**, 155 (1992).

34. N. E. Sluchanko, V. V. Glushkov, S. V. Demishev et al., Physica B **378–380**, 773 (2006).

35. N. E. Sluchanko, A. V. Bogach, V. V. Glushkov et al., Zh. Eksp. Teor. Fiz. **133**, 154 (2007).

36. P. Coleman, P. W. Anderson, and T. V. Ramakrishnan, Phys. Rev. Lett. **55**, 414 (1985).

37. A. Fert and P. M. Levy, Phys. Rev. B **36**, 1907 (1987).

38. J. M. Mignot, P. A. Alekseev, K. S. Nemkovski et al., Phys. Rev. Lett. **94**, 247204 (2005).

39. K. S. Nemkovski, J. M. Mignot, P. A. Alekseev et al., Phys. Rev. Lett. **99**, 137204 (2007).

40. T. S. Al'tshuler, A. E. Al'tshuler, and M. S. Bresler, Zh. Eksp. Teor. Fiz. **93**, 111 (2001).

41. N. E. Sluchanko, V. V. Glushkov, B. P. Gorshunov et al., Phys. Rev. B **61**, 15, 9906 (2000).

42. E. V. Nefedova, P. A. Alekseev, J. M. Mignot et al., J. Sol. St. Chem. **179**, 2858 (2006).

43. V. V. Glushkov, I. B. Voskoboinikov, S. V. Demishev et al., Zh. Eksp. Teor. Fiz. **126**, 444 (2004).

44. B. P. Gorshunov, P. Haas, O. Ushakov et al., Phys. Rev. B **73**, 045207 (2006).

45. B. P. Gorshunov, A. S. Prokhorov, I. E. Spector et al., Zh. Eksp. Teor. Fiz. **103**, 897 (2006).

46. J. Ye, Y. B. Kim, A. J. Millis et al., Phys. Rev. Lett. **83**, 3737 (1999).

47. Y. B. Kim, P. Majumdar, A. J. Millis, and B. I. Shraiman, arXiv:cond-mat/9803350.

48. N. E. Sluchanko, D. N. Sluchanko, V. V. Glushkov et al., Pis'ma v Zh. Eksp. Teor. Fiz. **86**, 691 (2007).

49. A. V. Bogach, V. V. Glushkov, S. V. Demishev et al., Acta Phys. Polon. A **118**, 931 (2010).

50. N. A. Samarin, M. A. Anisimov, V. V. Glushkov et al., Sol. St. Phenom. **152/153**, 525 (2009).

51. M. A. Anisimov, V. V. Glushkov, S. V. Demishev et al., arXiv:cond-mat/1006.0124.

52. A. C. Beer, in *Solid State Physics*, Suppl. No. 4 *Research and Applications*, ed. by F. Seitz and D. Turnbull, Acad. Press, New York&London (1963), p. 103.

53. W. A. Reed and J. A. Markus, Phys. Rev. **126**, 1298 (1962).

54. P. I. Baranskii and V. V. Baidakov, Phys. Stat. Sol.(a) **23**, K177 (1974).

55. M. R. Koblischka, M. Winter, and U. Hartmann, Semicond. Sci. Technol. **20**, 681 (2007); I. Janecek and P. Vašek, arXiv:cond-mat/0306560.

56. N. E. Sluchanko, A. V. Bogach, V. V. Glushkov et al., Pis'ma v Zh. Eksp. Teor. Fiz. **88**, 366 (2008).

57. N. E. Sluchanko, A. V. Bogach, V. V. Glushkov et al., J. Phys.: Conf. Ser. **200**, 012189 (2010).

58. V. V. Glushkov, S. V. Demishev, I. V. Krivitskiy et al., Physica B **359–361C**, 1165 (2005).

59. D. N. Sluchanko, V. V. Glushkov, S. V. Demishev et al., Physica B **403**, 1268 (2008).

60. H. von Lohneysen, T. Pietrus, G. Portisch et al., Phys. Rev. Lett. **72**, 3262 (1994).

61. B. Bogenberger and H. von Lohneysen, Phys. Rev. Lett. **74**, 1016 (1995).

62. A. Rosch, A. Schroder, O. Stockert, and H. von Lohneysen, Phys. Rev. Lett. **79**, 159 (1997).

63. A. Schroder, G. Aeppli, E. Bucher et al., Phys. Rev. Lett. **80**, 5629 (1998).

64. O. Stockert, H. von Lohneysen, A. Rosch et al., Phys. Rev. Lett. **80**, 5627 (1998).

65. H. von Lohneysen, C. Pfleiderer, T. Pietrus et al., Phys. Rev. B **63**, 134411 (2001).

66. O. Stockert, F. Huster, A. Neubert et al., Physica B **312/313**, 458 (2002).

67. G. S. Stewart, Rev. Mod. Phys. **73**, 797 (2001).

68. C. M. Varma, Z. Nussinov, and W. van Saarloos, Phys. Rep. **361**, 267 (2002).

69. S. M. Stishov, Usp. Fiz. Nauk **174**, 853 (2004).

70. G. S. Stewart, Rev. Mod. Phys. **78**, 743 (2006).

71. G. M. Kavius, D. R. Noakes, N. Marcano et al., Physica B **326**, 398 (2003).

72. G. M. Kavius, D. R. Noakes, N. Marcano et al., Physica B **312/313**, 210 (2002).

73. Y. Takeda, M. Arita, M. Higashiguchi et al., Phys. Rev. B **73**, 033202 (2006).

74. H. von Lohneysen, A. Neubert, T. Pietrus et al., Eur. Phys. J. B **5**, 447 (1998).

75. K. Grube, W. H. Fietz, U. Tutsch et al., Phys. Rev. B **60**, 11947 (1999).

76. N. E. Sluchanko, A. V. Bogach, V. V. Glushkov et al., Zh. Eksp. Teor. Fiz. **135**, 766 (2009).

77. N. E. Sluchanko, A. V. Bogach, V. V. Glushkov et al., Pis'ma v Zh. Eksp. Teor. Fiz. **91**, 81 (2010).

78. T. S. Al'tshuler, Yu. V. Goryunov, M. S. Bresler et al., Phys. Rev. B **68**, 014425 (2003).

79. F. Iga, Y. Takakuwa, T. Takahashi et al., Sol. St. Comm. **50**, 903 (1984).

80. M. Kasaya, F. Iga, M. Takigawa, and T. Kasuya, J. Magn. Magn. Mater. **47/48**, 429 (1985).

81. O. Stockert, H. von Lohneysen, W. Schmidt et al., J. Low Temp. Phys. **161**, 55 (2010).